1. Introduction

Alzheimer's disease (AD) is a major cause for dementia and has been considered to be a distinct entity from vascular dementia. However, recent pieces of evidence indicate a contribution of chronic cerebral hypoperfusion to the pathogenesis of AD. Indeed, reduction of cerebral blood flow (CBF) has been shown in temporal, parietal, and frontal cortices in the patients with AD (Waldemar et al., 1994; Johnson et al., 1998). This reduction of CBF has been attributed to reduced cerebral metabolism previously and may represent neurovascular coupling in response to an impaired synaptic activity.

However, several lines of evidence indicate dysregulation of regional CBF in AD brains, independent from derangement of synaptic activity. A decrease of CBF is documented even at early stages, indicating a microcirculatory insufficiency before the onset of AD pathology (Prohovnik et al., 1988). In addition, vascular networks in the cerebral cortices of AD patients are damaged and may contribute to the decrease of CBF (De Jong et al., 1997; Farkas et al., 2000; Kitaguchi et al., 2007), although it remains unclear whether these capillary damages are secondary to amyloid β (Aβ) deposition. Finally, in AD brains, there are frequent white matter (WM) lesions and cortical microinfarctions (Suter et al., 2002; Kovari et al., 2007), which are attributed to chronic cerebral hypoperfusion. In concordance with this microvascular derangement in AD, epidemiological data have revealed that vascular factors including mid-life hypertension and hyperlipidemia, diabetes mellitus, apo E4 genotype, are common risks for both AD and vascular dementia (Skoog et al., 1996; Launer et al., 2000; Kalaria, 2002; Kivipelto et al., 2006). Taken together, one can hypothesize that vascular factors and chronic cerebral hypoperfusion may accelerate AD pathology and cognitive decline.

However, there have been no data on whether chronic cerebral ischemia accelerates Aβ deposition in vivo, because the appropriate animal models have not been available. For this purpose, we successfully established a mouse model of chronic cerebral hypoperfusion, which exhibits mild cerebral hypoperfusion for an extended period and subsequently shows WM lesions and working memory deficits (Shibata et al., 2004; Shibata et al., 2007; Nakaji et al., 2006). In the present study, we applied chronic cerebral hypoperfusion to APP-Tg mouse and tested a possible alteration of Aβ metabolism.

2. Results

2.1. Histological stainings and immunohistochemistry

In the BCAS-treated mice at the age of 6 months and later, the WM was rarefied in the corpus callosum, caudoputamen, internal capsule and *anterior commissure* using Klüver-Barrera staining (Figs. 1A and B). However, there were no foci of cerebral infarctions in the cerebral cortices and the hippocampus. Using immunohistochemistry for GFAP, astroglia were much more numerous in the cerebral cortices, hippocampus, and WM such as the corpus callosum in the BCAS-treated mice at ages of 6, 9, and 12 months, as compared to those in the sham-operated mice (Figs. 1C and D).

Amyloid β_{1-40} immunostaining was observed occasionally in the vessel walls at 6 months and thereafter both in the mice with and without chronic cerebral hypoperfusion (Fig. 2A and B), whereas there were no obvious immunoreactivities in the neuronal somata for $A\beta_{1-42}$. There was no specific staining for $A\beta_{1-40}$ and $A\beta_{1-42}$ without the primary antibodies, and in the sections from wild-type mice which were subjected to either sham operation or BCAS. In the BCAS-treated mice at ages of 6, 9, and 12 months, there were neurons intensely immunoreactive for $A\beta_{1-42}$ with perinuclear staining, which may suggest accumulation of the antigen in the Golgi apparatus and multivesicular bodies, as compared to the sham-operated mice (Figs. 2C–H).

The numerical density of neurons with intensely immunoreactive for $A\beta_{1-42}$ were estimated in the representative 10 fields of 0.18 mm^2 from the cerebral cortex either sham-operated or BCAS-treated mice at ages of 12 months. Fig. 3A indicates an increase of these neurons with intense immunoreactivities for $A\beta_{1-42}$. The mouse model of chronic cerebral hypoperfusion does not exhibit focal necrosis *or atrophy* in the gray matter (Shibata et al., 2007). Similarly, in the gray matter, we did not observe any focal necrosis in the present study, but apoptotic cells significantly increased in number in the hippocampal CA1 and cerebral cortices even at ages of 12 months after BCAS (Figs. 3A and B). Therefore, one can postulate that intracellular accumulation of Aβ affects cellular metabolism and may have some relationship to apoptotic cell death, although it remains unclear whether these apoptotic neurons lead to significant reduction of neuronal density.

In the WM, including pencil fibers of the caudoputamen, optic tract and internal capsules, there were varicose fibers that were immunoreactive to antibodies against $A\beta_{1-42}$, whereas those immunoreactive for $A\beta_{1-40}$ were rarely found (Figs. 4A–D). Accumulation of $A\beta_{1-40}$ and $A\beta_{1-42}$ in the neuropil appeared occasionally in mice at the age of 7 months and constantly at 10 months, either with or without chronic cerebral hypoperfusion. With the antibody against $A\beta_{1-42}$, the immunoreactivity appeared as focal deposits surrounded by fibrillary deposits, whereas those for $A\beta_{1-40}$ were restricted to the round focal deposits, although the significance of differential pattern of amyloid deposits remained unclear (Figs. 4E and F). There were no differences in the distribution of $A\beta_{1-40}$ and $A\beta_{1-42}$ between the short-period group at ages of 12 months and the long-period group.

2.2. Western blot and filter assay

BCAS-treated mice showed the tendency to have higher levels of Aβ ($n=3$, $p=0.071$) in the extracellular-enriched brain fraction, as shown in the littermate pairs (a), (b), and (c) in the upper row of Fig. 5A. However, it did not reach statistical significance after correction by β-actin band density.

Next, we tested whether any structural changes in Aβ can be observed in chronic cerebral hypoperfusion with filter assay using ϕ200-nm nitrocellulose membrane, on which only the protein structures larger than 200 nm in diameter can be blotted. To validate the effectiveness of filter assay in specifically detecting Aβ fibrils, Aβ fibrils were prepared from synthetic $A\beta_{1-42}$ in vitro and subjected to filter assay as well as SDS-PAGE followed by the blotting, using anti-total Aβ

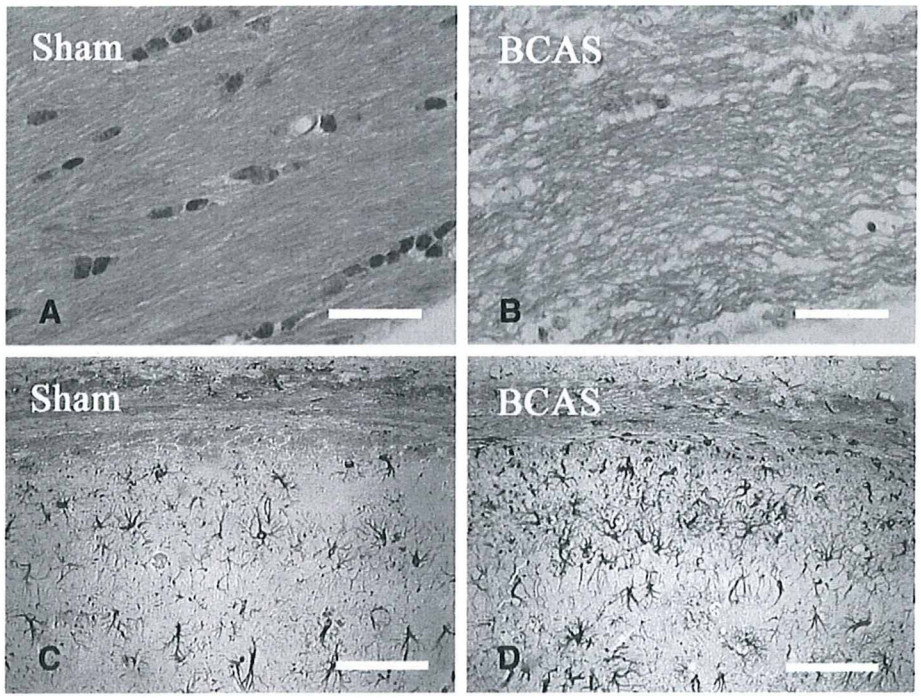

Fig. 1 – Photomicrographs of Klüver-Barrera staining (A, B) and immunohistochemistry for GFAP (C, D) in the corpus callosum (A, B) and the corpus callosum and hippocampal CA1 region (C, D) from the brains of sham-operated mice (A, C) and mice after chronic cerebral hypoperfusion (B, D). All mice were 12 months of age. Note the increase of GFAP-immunoreactive astroglia in both the corpus callosum and hippocampus. Scale bars indicate 50 μm.

(6E10) antibody (Fig. 5B). The Aβ fibrils formed after in vitro incubation were seen as high-molecular weight smear (Fig. 5B, asterisk [*]), which cannot be seen in the Aβ sample without incubation, whereas Aβ oligomers (Fig. 5B, asterisks [**]) and monomer (Fig. 5B, asterisks [***]) were detected with or without incubation. Conversely, in the filter assay, an Aβ-immunoreactive spot was seen only in the sample after incubation (Fig. 5B, bottom), indicating that monomers and oligomers had passed through the membrane.

Thus, we applied filter assay to the extracellular-enriched brain samples from the sham-operated and BCAS-treated mice. Interestingly, the Aβ-immmunoreactive spot density was increased *invariably* in the BCAS-treated mice, compared to the sham-operated mice (Fig. 5C), indicating that Aβ fibril formation was enhanced in the extracellular fraction after BCAS. Quantification of the spot density revealed that the increase was almost by 80% ($p=0.038$, $n=3$, Fig. 5D).

3. Discussion

In previous studies, increase of astroglia has been shown in the cerebral cortex and each part of the white matter in the BCAS-treated mice, along with rarefaction of the white matter (Shibata et al., 2004, 2007). The extent and distribution of glial activation in the present study correspond to those in previous reports and, therefore, indicate the same magnitude of ischemic insults after BCAS.

The altered metabolism of APP and Aβ has been indicated during in vitro hypoxia, and at multiple steps which favor the increase of APP and Aβ. Indeed, in human neuroblastoma cells, chronic hypoxia decreased the levels of α-secretase activity, which may upregulate Aβ production (Webster et al., 2002). In primary culture of neurons from human APP-Tg mice (Tg25769), hypoxia and glucose deprivation increased Aβ with a concomitant increase of γ-secretase and a delayed decrease of α-secretase, ADAM10 (Lee et al., 2006; Marshall et al., 2006). Hypoxia enhances the activity of β-secretase, the rate-limiting enzyme for Aβ production, in the cells expressing human APP695 (Zhang et al., 2007) and facilitates Aβ deposition and neuritic plaque formation in APP-Tg mice (Sun et al., 2006). More recently, neprilysin, metalloproteinase which degrades Aβ, has been shown to decrease in AD (Fisk et al., 2007).

In chronic cerebral ischemia, APP is accumulated in the neurites and soma of affected neurons (Wakita et al., 1992), being enhanced subcellularly in the endopalsmic reticulum and multivesicular bodies after transient global ischemia (Tomimoto et al., 1995). The increased cleavage of Aβ has been shown in a rat model of chronic cerebral hypoperfusion, but tissue deposition has not been demonstrated for Aβ (Bennet et al., 2000). In contrast, in focal cerebral ischemia, dense plaque-like APP deposits appear in the peri-infarct regions (van Groen et al., 2005).

These data collectively indicate that cerebral ischemia induces the abnormal metabolism of Aβ and may replicate the deposition of Aβ in AD. An altered metabolism in Aβ was shown in the present study after chronic cerebral hypoperfuion, but this mechanism remains unclear. β Secretase, β-site APP cleaving (BACE), is a membrane-bound aspartic protease, and the rate-limiting step in Aβ cleavage. Therefore, the Aβ

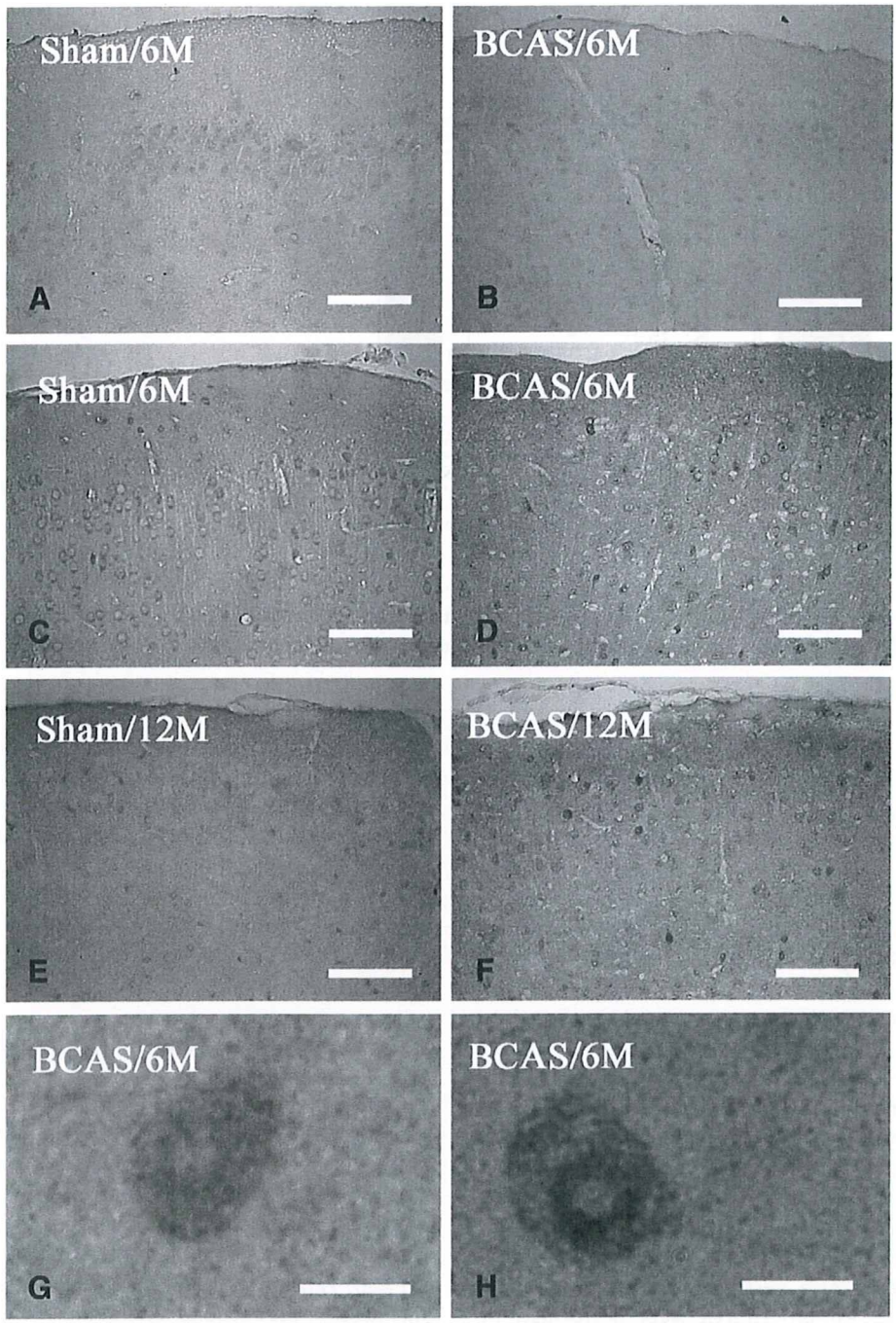

Fig. 2 – Photomicrographs of immunohistochemistry for $A\beta_{1-40}$ (A, B) and $A\beta_{1-42}$ (C–H) in the cerebral cortices. The mice were sham operated (A, C, E) and BCAS treated (B, D, F–H), and sacrificed at 6 months of age (A–D, G, H) and 12 months (E, F). Note that there are scattered intensely immunoreactive neurons, with enhanced immunostaining in the perinuclear regions. These neurons (H) were admixed with the neurons without perinuclear staining (G) in the cerebral cortices of BCAS-treated mice. Scale bars indicate 200 μm (A–F) and 10 μm (G, H).

load has been correlated with an increase in BACE activity in AD (Yang et al., 2003; Li et al., 2004; Chiocco et al., 2004; Johnston et al., 2005; Leuba et al., 2005). In aged APP-Tg mice, BACE was upregulated in the astroglia near amyloid plaques, suggesting that there may be Aβ production in the astroglia (Rossner et al., 2001). More recently, dysregulation in the inter-compartmental transport of soluble Aβ has also been reported in AD with an increase in the receptors for advanced glycation end products (RAGE), thus transporting Aβ into the brain, and a decrease of low-density receptor-related protein (LRP)-1, which transports Aβ outside of the brain (Donahue et al., 2006). Chronic cerebral hypoperfusion may affect each of these processes of Aβ metabolism, and the exact mechanisms should be indicated in the future study.

Finally, it remains to be addressed in the future whether chronic cerebral hypoperfusion induces the abnormal

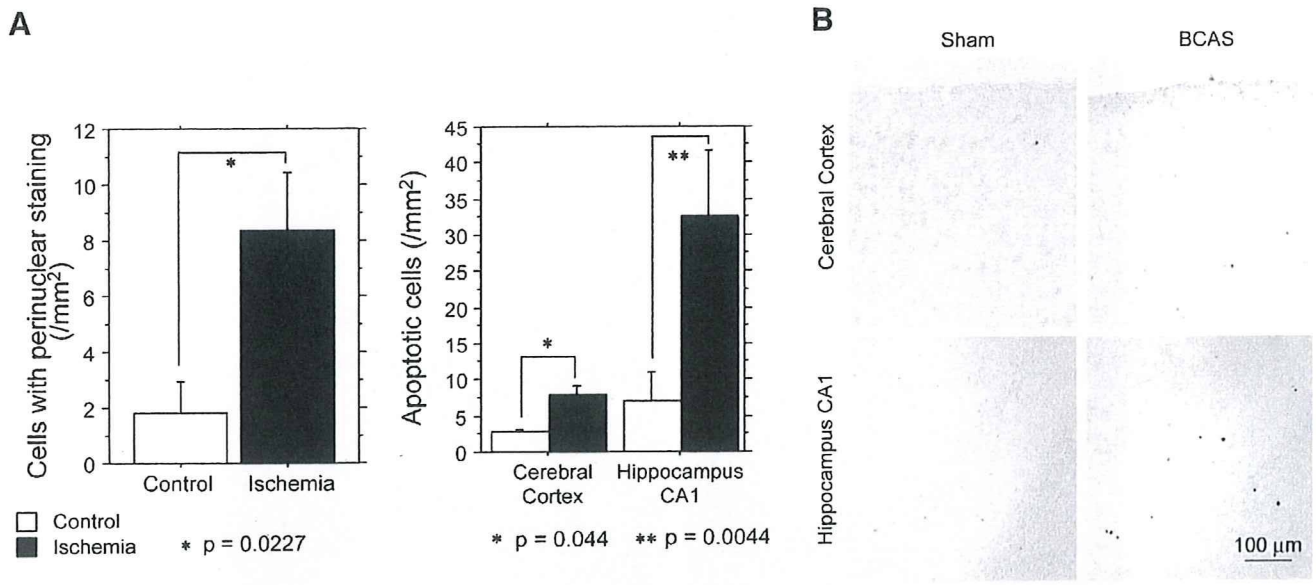

Fig. 3 – (A) Bar graphs showing the numerical density of cells with perinuclear staining and apoptotic cells. (B) Photomicrographs of TUNEL staining in the cerebral cortex and hippocampus in either sham-operated or BCAS-treated mice at 12 months of age.

phosphorylation of tau protein (Ikeda et al., 1998) and consequently accelerates synaptic dysfunction and cognitive deficits, since the Aβ load does not necessarily predict the magnitude of cognitive impairment (Giannakopoulos et al., 2003).

4. Experimental procedures

4.1. *Animals and treatments*

We used human APP-Tg mice overexpressing the familial AD-linked mutation carrying a mutant form of the human APP bearing the both Swedish (K670N/M671L) and the Indiana (V717F) mutations (APPSw*Ind*) (Mucke et al., 2000), which has been imported from the Jackson Laboratory (USA). Mice were screened for transgene expression by PCR, and heterozygous mice were mated with nontransgenic C57BL/6J mice. All male heterozygous transgenic mice were given free access to food and water *ad libitum*. All procedures were performed in accordance with the guidelines for animal experimentation from the ethical committee of Kyoto University.

These mice were anesthetized with sodium pentobarbital intraperitoneally. Through a midline cervical incision, both common carotid arteries (CCAs) were exposed and freed from their sheaths. The microcoils, which were made of piano wire with an inner diameter of 0.18 mm, were constructed in Sawane Spring Co. (Japan). This microcoil was twined by rotating around the right CCA. After 30 min, another microcoil was twined around the left CCA. For the sham operation, the CCAs of the animals were exposed, but the microcoils were not twined.

Comparisons were then performed between APPSw*Ind* transgenic mice and their littermates. At 5, 8, and 11 months of age, littermates of APP-Tg mice were subjected to either sham operation or bilateral carotid artery stenosis (BCAS) using microcoils (short-period group). One month after the sham operation or BCAS, these animals were examined. To test the effects of duration of chronic cerebral hypoperfusion, another batch of littermates of the APP-Tg mice were subjected to either sham operation or BCAS at 3 months of ages and were examined in the same manner after the survival for 9 months (long-period group). The long-period group was then compared to those operated at 11 months and sacrificed at 12 months.

4.2. *Histopathology and immunohistochemistry*

All animals were euthanized at 1 month and perfused transcardially with 0.01 mol/L phosphate-buffered saline (PBS) followed by 4% paraformaldehyde and 0.2% picric acid in 0.1 mol/L PBS (pH 7.4). The brains were removed and coronal brain blocks were postfixed for 24 h in 4% paraformaldehyde in 0.1 M PBS (pH 7.4) and then stored in 20% sucrose in 0.1 M PB (pH 7.4). Paraffin-embedded tissue was sectioned at 6-μm thickness. These sections were stained with hematoxylin and eosin (H & E) for examination of overall morphology and Klüver-Barrera staining for examination of the WM lesions.

For immunohistochemistry, the paraffin sections were incubated overnight at 4 °C with anti-glial fibrillary acidic protein (GFAP; Dakopatts, Denmark; diluted 1:1000). These sections were incubated with biotinylated anti-mouse IgG (Vector Laboratories, USA; diluted 1:200), and subsequently with avidin-biotin complex solution (Vector Laboratories; diluted 1:100). After each reaction, the sections were rinsed for 15 min with 0.1 M PBS. Finally, the immunoreaction products were visualized with a solution of 0.02% 3, 3′-diaminobenzidine tetrahydrochloride (DAB) and 0.005% H_2O_2 in 0.05 M Tris buffer (pH 7.6). Immunohistochemistry for $A\beta_{1-40}$ and $A\beta_{1-42}$ was performed using Aβ staining kit (Dakoppatts, Denmark) according to the manufacturer's recommendation.

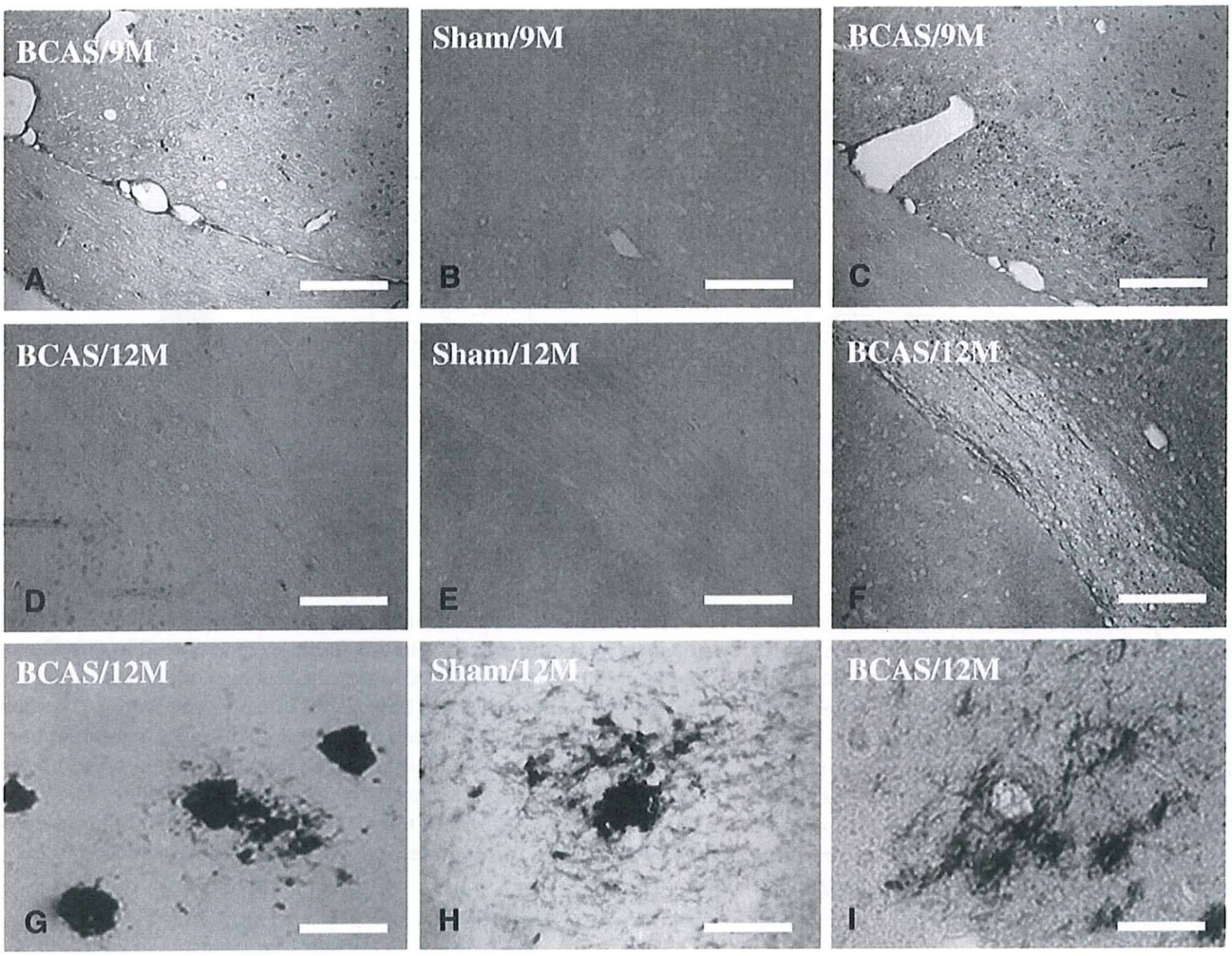

Fig. 4 – Photomicrographs of the immunohistochemistry for $A\beta_{1-40}$ (A, D, G) and $A\beta_{1-42}$ (B, C, E, F, H, I) in the internal capsule and optic tract (A–F) and the hippocampal CA3 region (G–I). Mice were sham treated (B, E, H) and BCAS treated (A, C, D, F, G, I) and sacrificed at 9 months of age (A–C) and 12 months (D–I). Scale bars indicate 500 μm (A–F) and 100 μm (G–I).

TUNEL staining was performed using the Apoptag in situ kit obtained from Oncor (Gaithersberg, MD, USA). After immersion in an equilibration buffer for 5 min, the sections were incubated with TdT and dUTP-digoxigenin in a humidified chamber at 37 °C for 1 h, and then incubated in the stop/wash buffer for 30 min. The sections were washed with 0.1 M PBS and incubated with an anti digoxigenin-peroxidase solution for 30 min. The sections were colorized with DAB-H_2O_2 solution as described above.

4.3. *Protein extraction*

The protein samples for Western blotting and the filter assay were extracted according to the method proposed by Lesne et al. (2006). Briefly, hemi-forebrains were harvested in 500 μL of solution containing 50 mM Tris–HCl (pH 7.6), 1% NP-40, 150 mM NaCl, 2 mM EDTA, 0.1% SDS, 1 mM phenylmethylsulfonyl fluoride (PMSF), and a protease inhibitor cocktail (Sigma, USA). Soluble, extracellular-enriched proteins were collected from mechanically homogenized lysates (1 mL syringe, gauge 20 needle [10 repeats]) following centrifugation for 5 min at 3000 rpm. The protein concentration of the samples was measured according to the Bradford (1976) method and equal amount of protein was subjected to Western blotting or filter assay.

4.4. *Western blotting and filter assay*

To examine the changes of APP metabolism in chronic cerebral hypoperfusion, we extracted the extracellular-enriched proteins from the brains of either sham-operated or BCAS-treated mice according to the protocol by Lesne et al., (2006). These mice were operated at the age of 8 months and sacrificed at the age of 9 months. Three pairs (pairs (a), (b), and (c)) of sham-operated or BCAS-treated mice were used for the analysis. Samples containing equal amounts of protein were diluted by Tricine SDS sample buffer (2×) (Invitrogen, USA) and electrophoresed on a 10%–20% Tricine gel (Invitrogen) in Tricine SDS Running Buffer (Invitrogen) according to the manufacturers' recommendation. Immunoblotting was performed by transferring the proteins to a PVDF membrane, blocking this membrane with 5% skimmed milk in Tris–HCl-buffered saline containing 1% TritonX-100 (TBS-T), and incubated with the primary antibody (6E10, Sigma; diluted

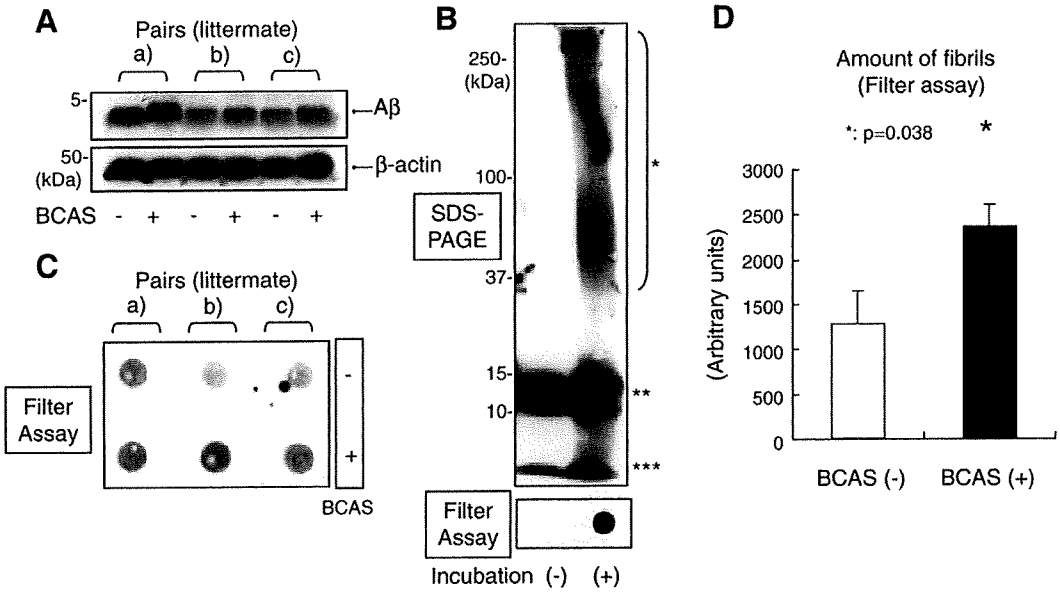

Fig. 5 – (A) Western blot of Aβ in the extracellular-enriched fraction of mouse brains using the anti-total Aβ (6E10) antibody. The lower panel indicates the bands of β-actin, which was used as a loading control. The Aβ fibrils were prepared in vitro from synthetic $Aβ_{1–42}$ and subjected to SDS-PAGE analysis (upper panel). (B) The Aβ fibril was seen as a high-molecular weight smear (*) after incubation. The Aβ oligomers (**) and monomer (***) bands were seen both before and after incubation. The filter assay (bottom panel) demonstrated an Aβ immunopositive spot only after incubation, indicating that the Aβ monomer and oligomers passed through the membrane pore and failed to be blotted onto the membrane. (C) Extracellular-enriched protein samples obtained from brains of either BCAS-treated mice or sham-operated littermates were subjected to the filter assay. The Aβ-immunoreactive spot density was increased in the samples from BCAS-treated mice, as compared to their sham-operated littermates. (D) Statistical analysis of Aβ-immunoreactive spot density. The spot density was significantly increased in the samples obtained the BCAS-treated mice ($p=0.038$, $n=3$).

1:1000) in overnight at 4 °C. The membranes were then incubated with a HRP-linked anti-mouse IgG secondary antibody (GE Healthcare, UK; diluted 1:100) for 1 h at room temperature. The specific reaction was visualized, using the ECL method (GE Healthcare).

Protein samples from the brains of transgenic mice were subjected to vacuum filtration through a 96-well dot blot apparatus (Bio-Rad Laboratories, USA) containing ϕ200-nm nitrocellulose membranes. The resultant membranes were then incubated with primary antibody (6E10; diluted 1:1000) at 4 °C overnight. The membranes were then blocked by TBS-T containing 5% skim milk, and incubated with HRP-linked anti-mouse IgG secondary antibody (GE Healthcare; diluted 1:100) for 1 h. The membranes were developed with the ECL Western Blotting Analysis System (GE Healthcare).

Aβ fibrils for the positive control of the filter assay were prepared from synthetic $Aβ_{1–42}$ (Bachem AG, Switzerland). $Aβ_{1–42}$ was dissolved and brought to 100 μM in 0.1 M HCl and incubated at 37 °C, 24 h, for preparation of fibrils. Control Aβ monomer was dissolved in DMSO (100 μM) and used immediately after preparation. The samples were diluted by PBS into 1 μM and subjected to filter assay.

4.5. *Statistical analysis*

Data were expressed as mean±SEM except when otherwise noted. Statistical analyses were carried out by a one-way ANOVA followed by post hoc Fisher protected least significant differences test. A value of $p<0.05$ was considered statistically significant. Spots density obtained by the filter assay was quantified by the NIH image analyzer. All values are given in means±SD. Comparisons were performed using a paired Student's *t*-test. A $p<0.05$ was considered to indicate a significant difference.

Acknowledgments

This work was supported by a grant-in-aid for scientific research (C) (18590936) from the Japanese Ministry of Education, Culture, Sports and Technology. This study is a part of joint research, which is focusing on the development of the basis of technology for establishing COE for nano-medicine, carried out through Kyoto City Collaboration of Regional Entities for Advancing Technology Excellence assigned by Japan Science and Technology Agency (JST).

REFERENCES

Bennett, S.A., Pappas, B.A., Stevens, W.D., Davidson, C.M., Fortin, T., Chen, J., 2000. Cleavage of amyloid precursor protein elicited by chronic cerebral hypoperfusion. Neurobiol. Aging 21, 207–214.

Bradford, M.M., 1976. A rapid and sensitive method for the quantitation of microgram quantities of protein utilizing the principle of protein-dye binding. Anal. Biochem. 72, 248–254.

Chiocco, M.J., Kulnane, L.S., Younkin, L., Younkin, S., Evin, G., Lamb, B.T., 2004. Altered amyloid-beta metabolism and deposition in genomic-based beta-secretase transgenic mice. J. Biol. Chem. 279, 52535–52542.

De Jong, G.I., De Vos, R.A., Steur, E.N., Luiten, P.G., 1997. Cerebrovascular hypoperfusion: a risk factor for Alzheimer's disease? Animal model and postmortem human studies. Ann. N. Y. Acad. Sci. 826, 56–74.

Donahue, J.E., Flaherty, S.L., Johanson, C.E., Duncan III, J.A., Silverberg, G.D., Miller, M.C., Tavares, R., Yang, W., Wu, Q., Sabo, E., Hovanesian, V., Stopa, E.G., 2006. RAGE, LRP-1, and amyloid-beta protein in Alzheimer's disease. Acta. Neuropathol. (Berl). 112, 405–415.

Farkas, E., De Jong, G.I., Apro, E., De Vos, R.A., Steur, E.N., Luiten, P.G., 2000. Similar ultrastructural breakdown of cerebrocortical capillaries in Alzheimer's disease, Parkinson's disease, and experimental hypertension. What is the functional link. Ann. N. Y. Acad. Sci. 903, 72–82.

Fisk, L., Nalivaeva, N.N., Boyle, J.P., Peers, C.S., Turner, A.J., 2007. Effects of hypoxia and oxidative stress on expression of neprilysin in human neuroblastoma cells and rat cortical neurons and astrocytes. Neurochem. Res. 32, 1741–1748.

Giannakopoulos, P., Herrmann, F.R., Bussiere, T., Bouras, C., Kovari, E., Perl, D.P., Morrison, J.H., Gold, G., Hof, P.R., 2003. Tangle and neuron numbers, but not amyloid load, predict cognitive status in Alzheimer's disease. Neurology 60, 1495–1500.

Ikeda, K., Akiyama, H., Arai, T., Kondo, H., Haga, C., Iritani, S., Tsuchiya, K., 1998. Alz-50/Gallyas-positive lysosome-like intraneuronal granules in Alzheimer's disease and control brains. Neurosci. Lett. 258, 113–116.

Johnson, K.A., Jones, K., Holman, B.L., Becker, J.A., Spiers, P.A., Satlin, A., Albert, M.S., 1998. Preclinical prediction of Alzheimer's disease using SPECT. Neurology 50, 1563–1571.

Johnston, J.A., Liu, W.W., Todd, S.A., Coulson, D.T., Murphy, S., Irvine, G.B., Passmore, A.P., 2005. Expression and activity of beta-site amyloid precursor protein cleaving enzyme in Alzheimer's disease. Biochem. Soc. Trans. 33 (Pt 5), 1096–1100.

Kalaria, R., 2002. Similarities between Alzheimer's disease and vascular dementia. J. Neurol. Sci. 203-204, 29–34.

Kitaguchi, H., Ihara, M., Saiki, H., Takahashi, R., Tomimoto, H., 2007. Capillary beds are decreased in Alzheimer's disease, but not in Binswanger's disease. Neurosci. Lett. 417, 128–131.

Kivipelto, M., Ngandu, T., Laatikainen, T., Winblad, B., Soininen, H., Tuomilehto, J., 2006. Risk score for the prediction of dementia risk in 20 years among middle aged people: a longitudinal, population-based study. Lancet. Neurol. 5, 735–741.

Kovari, E., Gold, G., Herrmann, F.R., Canuto, A., Hof, P.R., Bouras, C., Giannakopoulos, P., 2007. Cortical microinfarcts and demyelination affect cognition in cases at high risk for dementia. Neurology 68, 927–931.

Launer, L.J., Ross, G.W., Petrovitch, H., Masaki, K., Foley, D., White, L.R., Havlik, R.J., 2000. Midlife blood pressure and dementia: the Honolulu-Asia aging study. Neurobiol. Aging 21, 49–55.

Lee, P.H., Hwang, E.M., Hong, H.S., Boo, J.H., Mook-Jung, I., Huh, K., 2006. Effect of ischemic neuronal insults on amyloid precursor protein processing. Neurochem. Res. 31, 821–827.

Lesne, S., Koh, M.T., Kotilinek, L., Kayed, R., Glabe, C.G., Yang, A., Gallagher, M., Ashe, K.H., 2006. A specific amyloid-beta protein assembly in the brain impairs memory. Nature 440, 352–357.

Leuba, G., Wernli, G., Vernay, A., Kraftsik, R., Mohajeri, M.H., Saini, K.D., 2005. Neuronal and nonneuronal quantitative BACE immunocytochemical expression in the entorhinohippocampal and frontal regions in Alzheimer's disease. Dement. Geriatr. Cogn. Disord. 19, 171–183.

Li, R., Lindholm, K., Yang, L.B., Yue, X., Citron, M., Yan, R., Beach, T., Sue, L., Sabbagh, M., Cai, H., Wong, P., Price, D., Shen, Y., 2004. Amyloid beta peptide load is correlated with increased beta-secretase activity in sporadic Alzheimer's disease patients. Proc. Natl. Acad. Sci. U.S.A. 101, 3632–3637.

Marshall, A.J., Rattray, M., Vaughan, P.F., 2006. Chronic hypoxia in the human neuroblastoma SH-SY5Y causes reduced expression of the putative alpha-secretases, ADAM10 and TACE, without altering their mRNA levels. Brain Res. 1099, 18–24.

Mucke, L., Masliah, E., Yu, G.Q., Mallory, M., Rockenstein, E.M., Tatsuno, G., Hu, K., Kholodenko, D., Johnson-Wood, K., McConlogue, L., 2000. High-level neuronal expression of abeta 1-42 in wild-type human amyloid protein precursor transgenic mice: synaptotoxicity without plaque formation. J. Neurosci. 20, 4050–4058.

Nakaji, K., Ihara, M., Takahashi, C., Itohara, S., Noda, M., Takahashi, R., Tomimoto, H., 2006. Matrix metalloproteinase-2 plays a critical role in the pathogenesis of white matter lesions after chronic cerebral hypoperfusion in rodents. Stroke 37, 2816–2823.

Prohovnik, I., Mayeux, R., Sackeim, H.A., Smith, G., Stern, Y., Alderson, P.O., 1988. Cerebral perfusion as a diagnostic marker of early Alzheimer's disease. Neurology 38, 931–937.

Rossner, S., Apelt, J., Schliebs, R., Perez-Polo, J.R., Bigl, V., 2001. Neuronal and glial beta-secretase (BACE) protein expression in transgenic Tg2576 mice with amyloid plaque pathology. J. Neurosci. Res. 64, 437–446.

Skoog, I., Lernfelt, B., Landahl, S., Palmertz, B., Andreasson, L.A., Nilsson, L., Persson, G., Oden, A., Svanborg, A., 1996. 15-year longitudinal study of blood pressure and dementia. Lancet 347, 1141–1145.

Sun, X., He, G., Qing, H., Zhou, W., Dobie, F., Cai, F., Staufenbiel, M., Huang, L.E., Song, W., 2006. Hypoxia facilitates Alzheimer's disease pathogenesis by up-regulating BACE1 gene expression. Proc. Natl. Acad. Sci. U.S.A. 103, 18727–18732.

Suter, O.C., Sunthorn, T., Kraftsik, R., Straubel, J., Darekar, P., Khalili, K., Miklossy, J., 2002. Cerebral hypoperfusion generates cortical watershed microinfarcts in Alzheimer disease Stroke 33, 1986–1992.

Shibata, M., Ohtani, R., Ihara, M., Tomimoto, H., 2004. White matter lesions and glial activation in a novel mouse model of chronic cerebral hypoperfusion. Stroke 35, 2598–2603.

Shibata, M., Yamasaki, N., Miyakawa, T., Kalaria, R.N., Fujita, Y., Ohtani, R., Ihara, M., Takahashi, R., Tomimoto, H., 2007. Selective impairment of working memory in a mouse model of chronic cerebral hypoperfusion. Stroke 38, 2826–2832.

Tomimoto, H., Akiguchi, I., Wakita, H., Nakamura, S., Kimura, J., 1995. Ultrastructural localization of amyloid protein precursor in the normal and postischemic gerbil brain. Brain Res. 672, 187–195.

van Groen, T., Puurunen, K., Maki, H.M., Sivenius, J., Jolkkonen, J., 2005. Transformation of diffuse beta-amyloid precursor protein and beta-amyloid deposits to plaques in the thalamus after transient occlusion of the middle cerebral artery in rats. Stroke 36, 1551–1556.

Wakita, H., Tomimoto, H., Akiguchi, I., Ohnishi, K., Nakamura, S., Kimura, J., 1992. Regional accumulation of amyloid beta/A4 protein precursor in the gerbil brain following transient cerebral ischemia. Neurosci. Lett. 146, 135–138.

Waldemar, G., Bruhn, P., Kristensen, M., Johnsen, A., Paulson, O.B., Lassen, N.A., 1994. Heterogeneity of neocortical cerebral blood flow deficits in dementia of the Alzheimer type: a [99mTc]-d, l-HMPAO SPECT study. J. Neurol. Neurosurg. Psychiatry 57, 285–295.

Webster, N.J., Green, K.N., Peers, C., Vaughan, P.F., 2002. Altered processing of amyloid precursor protein in the human neuroblastoma SH-SY5Y by chronic hypoxia. J. Neurochem. 83, 1262–1271.

Yang, L.B., Lindholm, K., Yan, R., Citron, M., Xia, W., Yang, X.L., Beach, T., Sue, L., Wong, P., Price, D., Li, R., Shen, Y., 2003. Elevated beta-secretase expression and enzymatic activity detected in sporadic Alzheimer disease. Nat. Med. 9, 3–4.

Zhang, X., Zhou, K., Wang, R., Cui, J., Lipton, S.A., Liao, F.F., Xu, H., Zhang, Y.W., 2007. Hypoxia-inducible factor 1alpha (HIF-1alpha)-mediated hypoxia increases BACE1 expression and beta-amyloid generation. J. Biol. Chem. 282, 10873–10880.

BRAIN RESEARCH 1279 (2009) 139–146

available at www.sciencedirect.com

ScienceDirect

www.elsevier.com/locate/brainres

BRAIN RESEARCH

Research Report

Edaravone, a free radical scavenger, mitigates both gray and white matter damages after global cerebral ischemia in rats

Kozue Kubo[a], *Shinichi Nakao*[a,*], *Sachiko Jomura*[a], *Sachiyo Sakamoto*[a], *Etsuko Miyamoto*[a], *Yan Xu*[b], *Hidekazu Tomimoto*[c], *Takefumi Inada*[a], *Koh Shingu*[a]

[a]*Department of Anesthesiology, Kansai Medical University, Osaka, Japan*
[b]*Departments of Anesthesiology, Pharmacology, and Structural Biology, University of Pittsburgh School of Medicine, Pittsburgh, PA Pennsylvania, USA*
[c]*Department of Neurology, School of Medicine, Mie University, Mie, Japan*

ARTICLE INFO

Article history:
Accepted 25 April 2009
Available online 3 May 2009

Keywords:
Cardiac arrest
Global cerebral ischemia
Edaravone
Free radical scavenger
White matter damage

ABSTRACT

Recent studies have shown that similar to cerebral gray matter (mainly composed of neuronal perikarya), white matter (composed of axons and glias) is vulnerable to ischemia. Edaravone, a free radical scavenger, has neuroprotective effects against focal cerebral ischemia even in humans. In this study, we investigated the time course and the severity of both gray and white matter damage following global cerebral ischemia by cardiac arrest, and examined whether edaravone protected the gray and the white matter. Male Sprague–Dawley rats were used. Global cerebral ischemia was induced by 5 min of cardiac arrest and resuscitation (CAR). Edaravone, 3 mg/kg, was administered intravenously either immediately or 60 min after CAR. The morphological damage was assessed by cresyl violet staining. The microtubule-associated protein 2 (a maker of neuronal perikarya and dendrites), the β amyloid precursor protein (the accumulation of which is a maker of axonal damage), and the ionized calcium binding adaptor molecule 1 (a marker of microglia) were stained for immunohistochemical analysis. Significant neuronal perikaryal damage and marked microglial activation were observed in the hippocampal CA1 region with little axonal damage one week after CAR. Two weeks after CAR, the perikaryal damage and microglial activation were unchanged, but obvious axonal damage occurred. Administration of edaravone 60 min after CAR significantly mitigated the perikaryal damage, the axonal damage, and the microglial activation. Our results show that axonal damage develops slower than perikaryal damage and that edaravone can protect both gray and white matter after CAR in rats.

* *Corresponding author.* 2-3-1 Shinmachi, Hirakata City, Osaka 573-1191, Japan. Fax: +81 72 804 2785.
E-mail address: nakaos@hirakata.kmu.ac.jp (S. Nakao).

Abbreviations: CAR, cardiac arrest and resuscitation; MAP2, microtubule-associated protein 2; βAPP, beta amyloid precursor protein; Iba-1, ionized calcium binding adaptor molecule 1; NDS, neurologic deficit score

0006-8993/$ – see front matter © 2009 Elsevier B.V. All rights reserved.
doi:10.1016/j.brainres.2009.04.045

1. Introduction

Transient global cerebral ischemia, the most common clinical feature of which is circulatory arrest, leads to severe neuronal damage in selectively vulnerable brain areas, such as the hippocampal CA1 region, medium-sized neurons in the striatum, and the neocortical neurons in layers 3, 5 and 6, in both experimental animals and humans (Horn and Schlote, 1992; Kirino, 1982; Petito et al., 1987; Pulsinelli et al., 1982). A number of promising neuroprotective drugs for cerebral ischemia, especially for focal ischemia, have been proposed for preclinical testing, but almost all of these drugs have been found disappointing in clinical trials (Gladstone et al., 2002). One of the reasons why these neuroprotective drugs do not demonstrate obvious clinical benefits is the fact that preclinical studies have concentrated exclusively on protection of cerebral gray matter, i.e., neuronal perikarya. However, damage of white matter, which is composed of myelinated axons and glias, specifically oligodendrocytes, following acute cerebral ischemia and the effects of neuroprotective drugs on white matter have been largely neglected (Gladstone et al., 2002). Protecting only neuronal perikarya from ischemic insults is of little benefit to maintain neuronal function if their axons are not being protected, and thus Dewar et al. (1999) have emphasized that "total brain protection", in which not only gray matter but also white matter should be protected, is important and necessary.

Cerebral white matter is as vulnerable to ischemic insults as cerebral gray matter (Pantoni et al., 1996), although the pathophysiology and mechanisms of white matter damage differ in certain ways from those of gray matter damage (Dewar et al., 1999; Gladstone et al., 2002). For example, glutamatergic NMDA receptors are not expressed in axons and oligodendrocytes. As a consequence, blockade of Na^+ channels and AMPA/kinate receptors is more important for white matter to maintain Ca^{2+} homeostasis during ischemia (Dewar et al., 1999). Actually, MK-801, which markedly reduces ischemic damage to neuronal perikarya, had no protective effect on axonal damage following middle cerebral artery occlusion (Yam et al., 2000).

There is increasing evidence that oxidative stress following ischemia-reperfusion contributes to neuronal damage (Liachenko et al., 2003). Edaravone (3-Methyl-1-phenyl-2-pyrazolin-5-one) is a free radical scavenger and clinically available in Japan (Yoneda et al., 2003). It has been demonstrated that edaravone has a neuroprotective effect on focal cerebral ischemia (Abe et al., 1988; Amemiya et al., 2005), while there is no consensus about edaravone's neuroprotective effect on global cerebral ischemia (Jin et al., 2002; Otani et al., 2005). To our knowledge, there is no report on edaravone's effect on cerebral white matter damage. We hypothesized that edaravone would be effective in protecting not only gray matter but also white matter against cerebral ischemia, because white matter is abundant in lipid which can be peroxidized following ischemia-reperfusion insults.

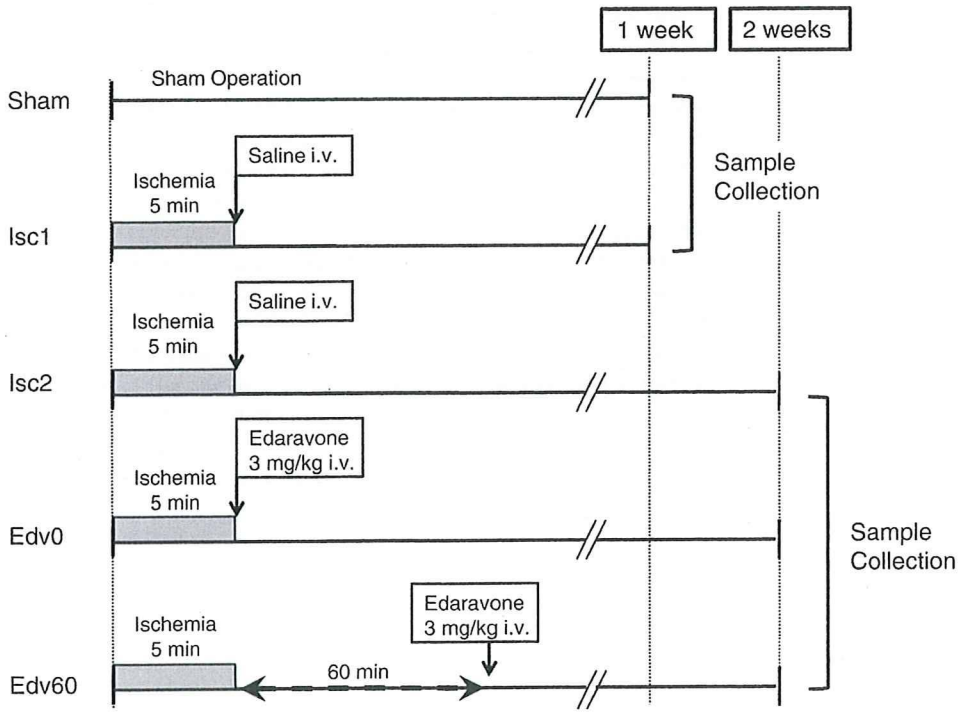

Fig. 1 – Experimental groups and protocol. This figure shows the schematic diagram depicting the experimental protocol. In Sham group, rats were subjected to the same surgical procedure but did not undergo cardiac arrest and resuscitation (CAR). In Isc1 and Isc2 groups, rats were subjected to 5 min cardiac arrest and treated with saline immediately after CAR. Rats in Edv0 and Edv60 groups were subjected to 5 min cardiac arrest and given 3 mg/kg edaravone intravenously immediately after CAR or 60 min after CAR, respectively. The rats in the Sham and the Isc1 groups were killed one week after CAR. Rats in the Isc2, Edv0, and Edv60 groups were killed two weeks after CAR.

The aim of this study was to investigate firstly, the time course and the severity of both gray and white matter damage following global cerebral ischemia after cardiac arrest and secondly, the effect of edaravone on reducing gray and white matter damage.

2. Results

2.1. *Physiological variables*

Fig. 1 shows the schematic diagram depicting the experimental protocol. Fifty rats were randomly assigned to one of 5 groups (in each group, $n=10$): Sham group, Isc1 group, Isc2 group, Edv0 group, and Edv60 group. Seven out of 50 rats (three rats in Isc1, two in Isc2, and two in Edv60 group) were excluded from the study because of massive bleeding during operation.

Table 1 summarizes the physiological variables before and after cardiac arrest and resuscitation (CAR). The pH, pO_2, pCO_2, and blood glucose were all within the normal physiological range before cardiac arrest and were not statistically different among the groups. Cardiac arrest time was not statistically different among the groups. After CAR, rats in the Isc2 group showed a significantly lower PaO_2 than the Sham group.

2.2. *Neurologic deficit scores*

Neurologic deficit scores (Jomura et al., 2007; Neumar et al., 1995) did not change after CAR in any group and showed almost full marks without paralysis (data is not shown).

2.3. *Time course and severity of neuronal damage induced by global cerebral ischemia*

Fig. 2 shows representative photomicrographs of the hippocampal CA1 region. In the Sham group, almost all neurons appeared healthy and showed round nuclei with dark cell bodies in cresyl violet staining (Fig. 2, A1). In contrast, there were numerous damaged neurons with pyknotic nuclei (the condensation of chromatin) and karyorhexis (the fragmentation of the nucleus) in the ischemic groups (Fig. 2, A2 and A3). The CAR caused a significant decrease in the number of surviving neurons in the hippocampal CA1 region (Fig. 3A). There was not significant difference between the number of surviving neurons in the Isc1 and Isc2 groups, which differed only in the recovery time, indicating that the neuronal perikaryal damage was fully established within a week after the CAR. Moreover, the ischemia caused an extensive decrease in microtubule-associated protein 2 (MAP2) expression in the hippocampal CA1 region (Fig. 2, B2 and B3). Fig. 3B shows the significant quantitative decrease in MAP2 expression in the CA1 region. The β amyloid precursor protein (βAPP) accumulation in the hippocampal CA1 region was quite low in the Sham and the Isc1 groups (Fig. 2, D1 and D2), but the global cerebral ischemia caused extensive βAPP accumulation 2 weeks after CAR (Fig. 2, D3 and Fig. 3C). Interestingly, βAPP accumulation following the global ischemia in axon-rich brain areas, such as the caudate putamen and the internal and external capsules, were sparse and some accumulation of βAPP was observed in the corpus callosum 2 weeks but not 1 week after CAR (Fig. 4, A2–3). Microglias were significantly activated at 1–2 weeks after CAR (Fig. 2, E1–3).

2.4. *Effects of edaravone on neuronal perikaryal damage and axonal damage*

Edaravone potently protected the brain against neuronal damage in the hippocampal CA1 region following global cerebral ischemia (Fig. 2, A4 and A5). The number of surviving neurons in the Edv60 group was significantly greater than in the Isc1 and Isc2 groups (Fig. 3 A). The number of surviving neurons in the Edv0 and Edv60 groups was not significantly different from that in the Sham group, indicating that edaravone restored the neuronal survivability to the control level (Fig. 3A). Furthermore, MAP2 staining confirmed that edaravone provided a significant neuroprotective effect against CAR (Fig. 2, B4 and B5). The bar graphs in Fig. 3B show that edaravone protected hippocampus against the MAP2 disruption nearly to the control level. In addition, edaravone significantly reduced the βAPP accumulation in the hippocampal CA1 region almost to the control (the Sham) level (Fig. 2, D1, D4, D5, and Fig. 3C). The βAPP accumulation in the corpus callosum was also attenuated by edaravone (Fig. 4, A3 and A4). The activation of microglias

Table 1 – Physiological variables.

		Weight (g)	Duration of cardiac arrest (min)	Before CAR				After CAR			
				pH	PaO_2 (FiO_2 0.6) (mm Hg)	$PaCO_2$ (mm Hg)	Glucose (mg/dl)	pH	PaO_2 (FiO_2 0.6) (mm Hg)	$PaCO_2$ (mm Hg)	Glucose (mg/dl)
Sham	($n=10$)	248±10	–	7.423±0.01	226±3	37±2	133±7	7.389±0.01	208±6	42±2	126±5
Isc1	($n=7$)	235±6	5.26±0.07	7.398±0.02	217±17	44±3	139±14	7.324±0.03	188±13	47±4	127±6
Isc2	($n=8$)	265±9	5.23±0.05	7.422±0.01	222±10	40±1	148±10	7.274±0.06	147±18[a]	55±9	131±9
Edv0	($n=10$)	245±6	5.20±0.04	7.420±0.02	219±21	40±1	171±11	7.335±0.04	157±20	49±6	133±7
Edv60	($n=8$)	248±3	5.09±0.07	7.452±0.01	256±15	37±1	156±11	7.359±0.02	152±12	43±2	135±11

CAR = cardiac arrest and resuscitation.
[a] $P<0.05$ compared with Sham group after CAR.

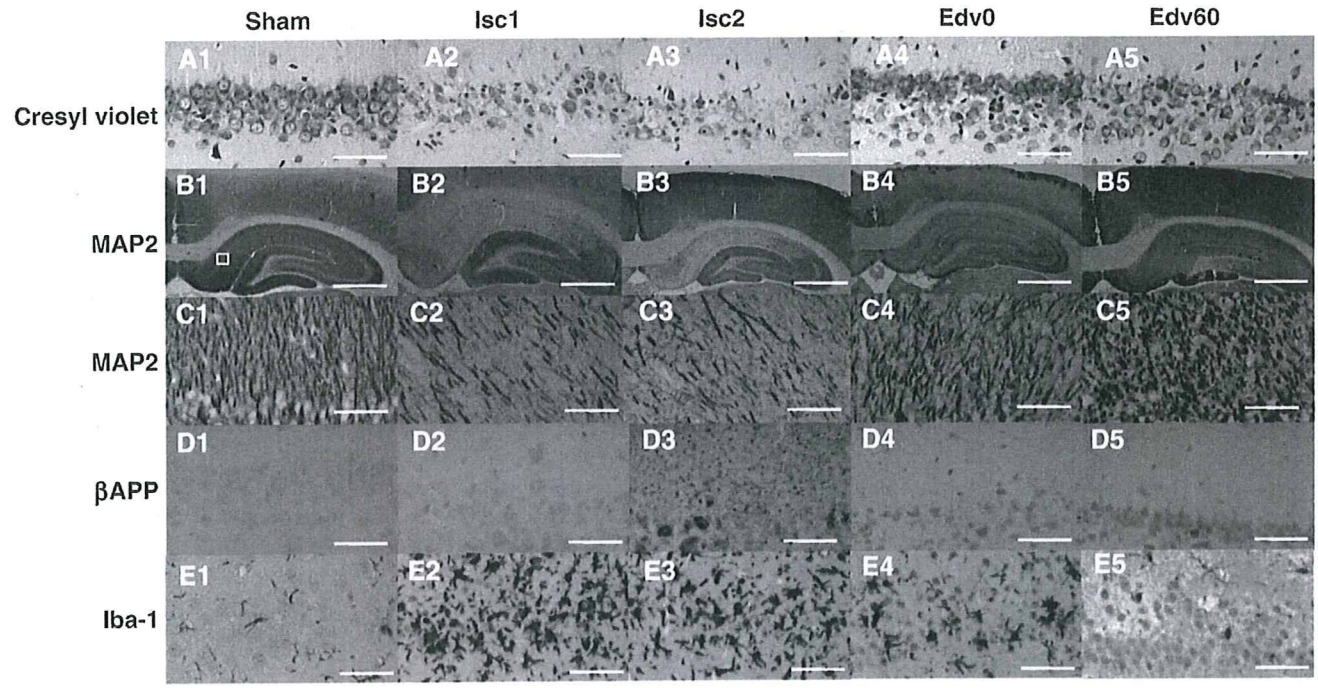

Fig. 2 – Histologic neuronal and axonal damages in the hippocampal CA1 region following global cerebral ischemia caused by cardiac arrest and resuscitation (CAR). Representative sections of cresyl violet staining (A1–5) and immunostained sections of MAP2 (B1–5 and C1–5), βAPP (D1–5), and Iba-1 (E1–5) in the CA1 in the Sham, Isc1, Isc2, Edv0, and Edv60 groups are depicted. A1: Normal pyramidal neurons in the Sham group. A2 and A3: Typical appearance of neuronal damage 1 week (Isc1) and 2 weeks (Isc2) after CAR, respectively. A4 and A5: Reduction of neuronal damage by edaravone administered immediately (Edv0) and 60 min (Edv60) after CAR, respectively. B1: Normal MAP2 expression in the Sham group. A white square shows the region of predetermined area for the neuronal perikaryal and axonal damages evaluation. B2 and B3: Extensive decrease in MAP2 expression after CAR in the Isc1 and Isc2 groups, respectively. B4 and B5: Mitigation of decrease in MAP2 expression by edaravone in the Edv0 and Edv60 groups. C: MAP2 expression as in B at a higher magnification. D1 and D2: Normal detection level of the βAPP accumulation in the Sham and Isc1 groups, respectively, one week after CAR. D3: Extensive granular βAPP deposition 2 weeks after CAR in the Isc2 group. D4 and D5: Mitigation of βAPP accumulation in the edaravone-treated groups. E1: Scattered ramified microglias are found in the Sham group. E2 and E3: Dense accumulation of ameboid microglias 1 week and 2 weeks after CAR. E4: Microglial activation is slightly suppressed by edaravone administered immediately after CAR. E5: Microglial activation is markedly suppressed by edaravone administered 60 min after CAR. Scale Bar: 50 μm (A, C, D, and E); 1 mm (B).

was significantly suppressed by edaravone (Fig. 2, E4 and E5 and Fig. 3D).

3. Discussion

The novel findings of this study are that axonal (white matter) damage develops slower than neuronal perikaryal (gray matter) damage, and that edaravone exerts significant protection against not only gray matter damage but also white matter damage induced by global cerebral ischemia.

It has been demonstrated that damage to hippocampal pyramidal neurons is delayed and is generally not fully developed until 5–7 days after reperfusion in animal models of forebrain ischemia (Kirino, 1982; Pulsinelli et al., 1982). We confirmed that neuronal perikaryal damage in the hippocampal CA1 region was apparent and completed by 1 week after CAR, whereas axonal damage was absent one week after CAR and only becoming clearly evident 2 weeks after CAR. Based on these results, we recommend that, in *in vivo* studies, the observation period following cerebral ischemia should be extended to a minimum of 2 weeks. Otherwise it is difficult to assess the efficacy of a drug with a potential for so-called "total brain protection (Dewar et al., 1999)" against cerebral ischemia. In this study, we examined the neuronal perikaryal damage using both the conventional cresyl violet staining and the MAP2 immunohistochemistry. Neuronal perikarya and dendrites express MAP2, which binds to and stabilizes microtubules, and may help to regulate microtubule spacing (Matus, 1988). A loss of MAP2 expression can be used as a sensitive and reliable marker of neuronal damage (Arai et al., 1994; Kitagawa et al., 1989). To evaluate axonal damage, the accumulation of the βAPP was investigated. βAPP is usually produced within neurons at a concentration lying below the detection threshold (Beeson et al., 1994; Koo et al., 1990; Lin et al., 1999), and it accumulates in the axon, less often within the neuronal cell body, when the fast anterograde axonal transport is disrupted following brain damage, such as ischemia (Koo et al., 1990; Yam et al., 1998). It is generally

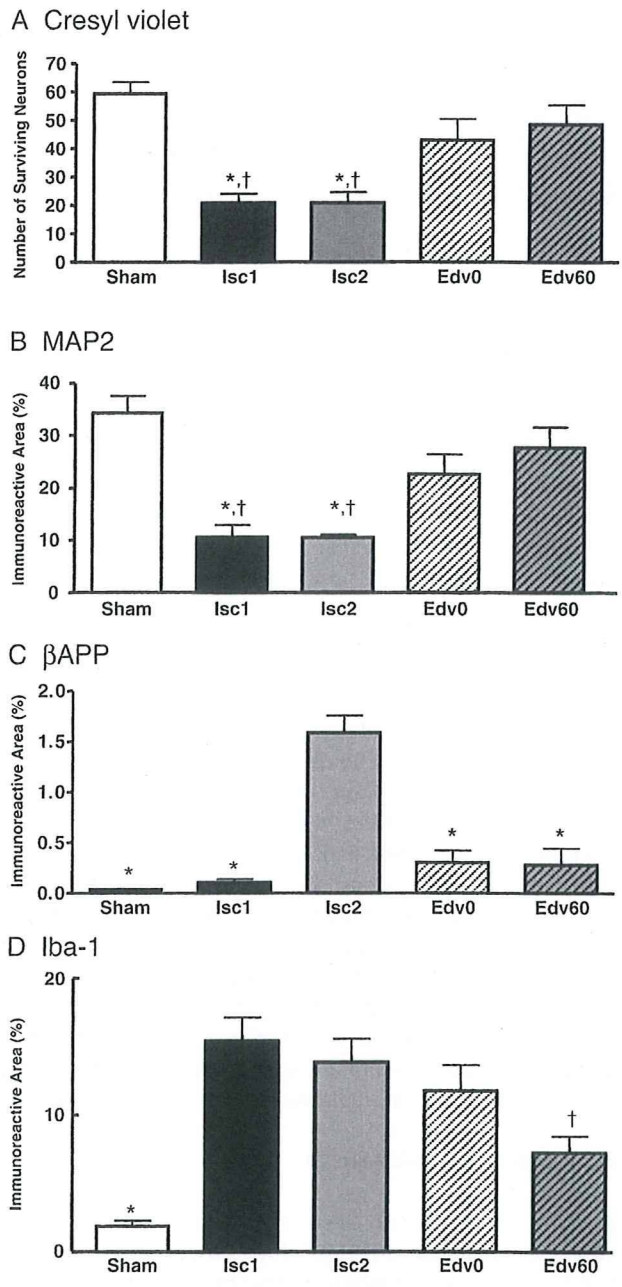

Fig. 3 – Quantified analyses of neuronal and axonal damages in the hippocampal CA1 region following global cerebral ischemia caused by cardiac arrest and resuscitation. A: The extent of neuronal perikaryal damage is quantified by counting the number of surviving neurons in a predetermined hippocampal CA1 region. *P<0.05 compared with the Sham group; †P<0.05 compared with the Edv60 group. B: Neuronal perikaryal damage, quantified by the percentage of MAP2 immunoreactive areas in a predetermined hippocampal CA1 region. *P<0.05 compared with the Sham group; †P<0.05 compared with the Edv60 group. C: Axonal damage, quantified by the percentage of the βAPP immunoreactive areas in a predetermined CA1. *P<0.05 compared with the Isc2 group. D: Microglial activation, quantified by the percentage of the Iba-1 immunoreactive areas in a predetermined hippocampal CA1 region. *P<0.05 compared with the Isc1 and Isc2 groups; †P<0.05 compared with the Isc1 and Isc2 groups.

accepted that βAPP accumulation is a good marker of axonal damage (Lin et al., 1999; van Groen et al., 2005).

White matter is traditionally considered less vulnerable than gray matter to ischemic insults (Marcoux et al., 1982). However, recent studies have shown that white matter is also vulnerable to ischemia (Dewar et al., 1999; Hirko et al., 2008; Pantoni et al., 1996; Pantoni and Garcia, 1997). Characteristic white matter lesions, sometimes in the absence of gray matter damage, are observed following expose of cyanide, or carbon monoxide (Pantoni et al., 1996). Such lesions also were observed after chronic cerebral hypoperfusion in a rat model (Miyamoto et al., 2001). In the present study, we cannot clarify whether the axonal damage in the CA1 is due to a direct effect of ischemia or a secondary damage of neuronal perikarya. However, we assume that the axonal damage is due to the direct effect of ischemia, because Wallerian degeneration in the mammalian central nervous system usually occurs very slowly, taking months to years to appear (Vargas and Barres, 2007). In addition, the evidence that there was a lot of βAPP accumulation in the CA1 stratum radiatum, which contains septal and commissural fibers from the contralateral hippocampus and Schaffer collateral fibers which are the projection forward from hippocampal CA3 region to the CA1 region, indicates that the axonal damage, at least partly, was induced directly by CAR but not secondarily after neuronal perikaryal damage because the CA3 neuronal perikarya were not damaged. Similar to βAPP accumulation in the CA1, βAPP accumulation in the corpus callosum, which is a representative white matter, was apparent at 2 weeks after the CAR and suppressed by edaravone.

Edaravone has been clinically used for the treatment of acute cerebral infarction in Japan since June 2001. Numerous animal studies have demonstrated the neuroprotective effects of edaravone against focal cerebral ischemia (Abe et al., 1988; Amemiya et al., 2005; Kawai et al., 1997), but there have been only a few reports which demonstrate that edaravone has neuroprotective effects against global (forebrain) cerebral ischemia (Otani et al., 2005; Watanabe et al., 1994; Yamamoto et al., 1997). We chose to use 3 mg/kg of edaravone, because this dose has been effective neuroprotection in rodent ischemic models (Abe et al., 1988; Amemiya et al., 2005; Watanabe et al., 1994). While the timing of edaravone administration was variable in previous studies (Abe et al., 1988; Amemiya et al., 2005; Otani et al., 2005; Watanabe et al., 1994), it was most often administered before or immediately after cerebral ischemia and reperfusion. In the present study, we demonstrated that edaravone, administered even 60 min after CAR, significantly protected not only gray matter but also white matter against ischemia.

Recent studies have shown that oxidative stress plays a pivotal role on brain damage following ischemia-reperfusion insult (Liachenko et al., 2003). Reactive oxygen species (ROS) induce lipid peroxidation, which can modify various cell membrane functions, such as neurotransmitter release and uptake, those of ion-channels, ion-motive ATPases, and GTP-binding proteins, leading to impaired mitochondrial function, resulting in apoptosis (Mattson, 1998). Our result showing greatly reduced axonal damage after edaravone treatment seems quite reasonable because white matter is abundant in lipid. The evidence that edaravone suppressed microglial

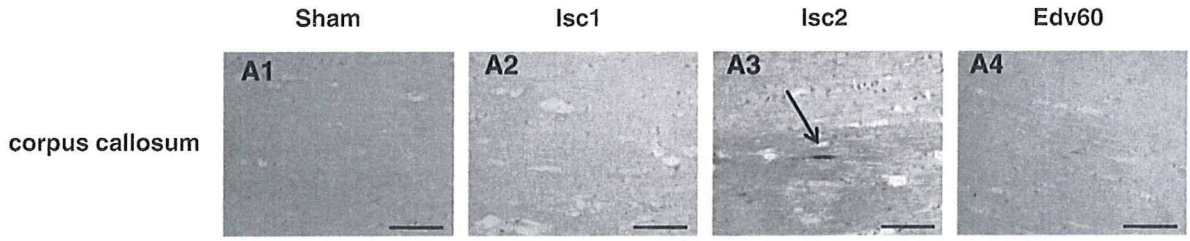

Fig. 4 – Axonal damage in the corpus callosum following global cerebral ischemia caused by cardiac arrest and resuscitation (CAR). βAPP immunoreactivity in the corpus callosum . A1: Absence of βAPP accumulation in the Sham group. A2: Little βAPP accumulation 1 week after CAR. A3: Positive staining of βAPP is seen in axons 2 weeks after CAR (arrow). A4: βAPP accumulation is suppressed by edaravone administered 60 min after CAR. Scale Bar: 50 μm.

activation suggests that edaravone exerted neuroprotection as a radical scavenger, because activated microglias produce ROS, which can cause neuronal damage and amplify the inflammatory response of microglias (Block et al., 2007). Although some authors have previously reported that free radical scavengers mitigate white matter damage in rodent brain ischemia models (Imai et al., 2001; Irving et al., 1997; Lin et al., 2006), they used radical scavengers other than edaravone and their cerebral ischemia models were different from ours. Moreover, as 60 min after CAR is a sufficiently long therapeutic time window in the clinical setting, edaravone seems to be a promising neuroprotective drug against global cerebral ischemia.

In conclusion, using a cardiac arrest model in rats, we demonstrated that white matter damage develops slower than gray matter damage in the hippocampal CA1 region, and edaravone, administered 60 min after CAR, significantly protected not only gray matter but also white matter. Our results indicate that the use of edaravone as a "total brain protection (Dewar et al., 1999)" drug against global cerebral ischemia in the clinical setting should be explored and evaluated.

4. Experimental procedures

4.1. *Animal model*

The study was approved by the Animal Research Committee at Kansai Medical University. Adult male Sprague–Dawley rats (Shimizu Laboratory Supplies Co., Ltd, Kyoto, Japan) weighing 210 to 290 g were used. Fifty rats were randomly assigned to one of five groups (Fig. 1). In the Sham group, rats were subjected to the same surgical procedure except for CAR. The Isc1 and Isc2 group rats were subjected to 5 min cardiac arrest and given physiologic saline intravenously immediately after CAR. The Edv0 and Edv60 group rats were subjected to 5 min cardiac arrest and treated with intravenous administration of 3 mg/kg edaravone immediately or 60 min after CAR, respectively.

Transient global ischemia was induced by the CAR technique as described previously (Jomura et al., 2007; Liachenko et al., 1998; Liachenko et al., 2001) with slight modifications. Under isoflurane anesthesia, rats were orotracheally intubated and mechanically ventilated. Rats were paralyzed by the intravenous administration of pancuronium bromide (1.5 mg/kg). Anesthesia was maintained with 1 to 2% isoflurane in 60% O_2 unless otherwise stated. The temporalis muscle temperature was monitored and maintained at 36.5± 0.5 °C during the surgical procedure using a feedback controlled heating blanket. Before the induction of cardiac arrest, the arterial blood pH and gases were measured using an i-STAT portable clinical analyzer 300F (FUSO pharmaceutical industries, Ltd., Osaka, Japan). The arterial blood glucose was measured using Medisafe Mini MS-GK03 V (Terumo Co., Tokyo, Japan).

Cardiac arrest was induced by an ultra-short-acting β_1-blocker, esmolol (7 mg), followed by the stoppage of mechanical ventilation. At this point, a sharp decrease in the mean arterial pressure to less than 10 mm Hg was considered as the induction of cardiac arrest. Strictly 5 min after the induction of cardiac arrest, resuscitation was performed by retrograde infusion of oxygenated blood mixed with a resuscitation mixture containing heparin (8 U/ml), sodium bicarbonate (0.05 mEq/ml), and epinephrine (8.5 μg/ml), at the same time ventilation was started with 100% O_2 for 10 min. The rats were ventilated for at least 60 min and were extubated when sustained spontaneous breathing was observed. Rats were returned to the cages and followed up for one or two weeks.

4.2. *Neurologic deficit scores*

Functional damage and recovery were evaluated using neurologic deficit scores (NDS), which ranges from a score of 500 indicating a neurologically normal rat, to 0 for brain death (Jomura et al., 2007; Neumar et al., 1995).

4.3. *Histology analysis*

Rats were observed for either 1 week (Sham and Isc1 groups) or 2 weeks (Isc2, Edv0, and Edv60 groups) after the surgery. Under deep isoflurane anesthesia, rats were perfused with buffered 10% formalin phosphate and the brains were extracted. The brain sections containing the dorsal hippocampal region were embedded in paraffin and sliced into 5-μm-thick coronal sections. The sections were stained with cresyl violet and the hippocampal CA1 regions were photographed. For immunohistochemical staining, brain sections were deparaffinized and incubated with mouse monoclonal antibodies against MAP2 (Sigma-Aldrich, St. Louis, MO) or βAPP (Zymed, South San Francisco, CA), or with a rabbit polyclonal antibody against Iba-1 (Wako Pure Chemical, Osaka, Japan). The

sections were subsequently incubated with biotinylated anti-mouse IgG for monoclonal antibodies or biotinylated anti-rabbit IgG for Iba-1 (Vector Laboratories, Burlingame, CA), and then incubated with an avidin-biotin peroxidase complex solution (Vector Laboratories). The immunoreactive products were visualized with a solution of 0.02% 3, 3′-diaminobenzidine tetrahydrochloride containing 0.005% H_2O_2 in 0.05 M Tris buffer (pH 7.6).

4.4. *Morphometry and statistical analysis*

The neuronal and axonal damages were determined in a predetermined area of 0.0374 mm^2 in the hippocampal CA1 region in each hemisphere (square in Fig. 2, B1). To quantify the histological damage, morphologically normal neurons stained with cresyl violet were counted by two observers blind to the treatment and showed as the number of surviving neurons. The βAPP, MAP2, and Iba-1 expression positive areas were calculated with the use of a computer-assisted image analysis system (NIH Image J) attached to a light microscope and a high-resolution color video camera (Miyamoto et al., 2001).

Statistical comparison of physiological variables, histological data, NDS, and body weight on the same day among groups was made by one-way analysis of variance (ANOVA) followed by the Bonferroni *post hoc* test using Graph Pad Prizm (GraphPad Software, Inc., San Diego, CA). All data were expressed as mean±SEM. A P value <0.05 was considered statistically significant.

Acknowledgments

This work was supported by a Grant-in-Aid for Scientific Research B-19791092 and C-19591825 from the Japan Society for the Promotion of Science. Yan Xu acknowledges the support from the National Institutes of Health of the United States (Grant # R01NS036124). Edaravone was kindly donated by Mitsubishi Tanabe Pharma Corporation (Osaka, Japan).

REFERENCES

Abe, K., Yuki, S., Kogure, K., 1988. Strong attenuation of ischemic and postischemic brain edema in rats by a novel free radical scavenger. Stroke 19, 480–485.

Amemiya, S., Kamiya, T., Nito, C., Inaba, T., Kato, K., Ueda, M., Shimazaki, K., Katayama, Y., 2005. Anti-apoptotic and neuroprotective effects of edaravone following transient focal ischemia in rats. Eur. J. Pharmacol. 516, 125–130.

Arai, T., Watanabe, K., Nakao, S., Mori, H., Murakawa, M., Mori, K., Tooyama, I., Kimura, H., Kojima, S., 1994. Effects of neopterin on ischemic neuronal damage in gerbils. Neurosci. Lett. 173, 107–110.

Beeson, J., Shelton, E., Chan, H., Gage, F., 1994. Differential distribution of amyloid protein precursor immunoreactivity in the rat brain studied by using five different antibodies. J. Comp. Neurol. 342, 78–96.

Block, M., Zecca, L., Hong, J., 2007. Microglia-mediated neurotoxicity: uncovering the molecular mechanisms. Nat. Rev. Neurosci. 8, 57–69.

Dewar, D., Yam, P., McCulloch, J., 1999. Drug development for stroke: importance of protecting cerebral white matter. Eur. J. Pharmacol. 375, 41–50.

Gladstone, D., Black, S., Hakim, A., 2002. Toward wisdom from failure: lessons from neuroprotective stroke trials and new therapeutic directions. Stroke 33, 2123–2136.

Hirko, A., Dallasen, R., Jomura, S., Xu, Y., 2008. Modulation of inflammatory responses after global ischemia by transplanted umbilical-cord matrix stem cells. Stem. Cells 26, 2893–2901.

Horn, M., Schlote, W., 1992. Delayed neuronal death and delayed neuronal recovery in the human brain following global ischemia. Acta Neuropathol. 85, 79–87.

Imai, H., Masayasu, H., Dewar, D., Graham, D., Macrae, I., 2001. Ebselen protects both gray and white matter in a rodent model of focal cerebral ischemia. Stroke 32, 2149–2154.

Irving, E., Yatsushiro, K., McCulloch, J., Dewar, D., 1997. Rapid alteration of tau in oligodendrocytes after focal ischemic injury in the rat: involvement of free radicals. J. Cereb. Blood Flow Metab. 17, 612–622.

Jin, Y., Mima, T., Raicu, V., Park, K., Shimizu, K., 2002. Combined argatroban and edaravone caused additive neuroprotection against 15 min of forebrain ischemia in gerbils. Neurosci. Res. 43, 75–79.

Jomura, S., Uy, M., Mitchell, K., Dallasen, R., Bode, C., Xu, Y., 2007. Potential treatment of cerebral global ischemia with Oct-4+ umbilical cord matrix cells. Stem. Cells 25, 98–106.

Kawai, H., Nakai, H., Suga, M., Yuki, S., Watanabe, T., Saito, K., 1997. Effects of a novel free radical scavenger, MCl-186, on ischemic brain damage in the rat distal middle cerebral artery occlusion model. J. Pharmacol. Exp. Ther. 281, 921–927.

Kirino, T., 1982. Delayed neuronal death in the gerbil hippocampus following ischemia. Brain Res. 239, 57–69.

Kitagawa, K., Matsumoto, M., Niinobe, M., Mikoshiba, K., Hata, R., Ueda, H., Handa, N., Fukunaga, R., Isaka, Y., Kimura, K., 1989. Microtubule-associated protein 2 as a sensitive marker for cerebral ischemic damage—immunohistochemical investigation of dendritic damage. Neuroscience 31, 401–411.

Koo, E., Sisodia, S., Archer, D., Martin, L., Weidemann, A., Beyreuther, K., Fischer, P., Masters, C., Price, D., 1990. Precursor of amyloid protein in Alzheimer disease undergoes fast anterograde axonal transport. Proc. Natl. Acad. Sci. U. S. A. 87, 1561–1565.

Liachenko, S., Tang, P., Hamilton, R., Xu, Y., 1998. A reproducible model of circulatory arrest and remote resuscitation in rats for NMR investigation. Stroke 29, 1229–1238 discussion 1238–9.

Liachenko, S., Tang, P., Hamilton, R., Xu, Y., 2001. Regional dependence of cerebral reperfusion after circulatory arrest in rats. J. Cereb. Blood Flow Metab. 21, 1320–1329.

Liachenko, S., Tang, P., Xu, Y., 2003. Deferoxamine improves early postresuscitation reperfusion after prolonged cardiac arrest in rats. J. Cereb. Blood Flow Metab. 23, 574–581.

Lin, B., Schmidt-Kastner, R., Busto, R., Ginsberg, M., 1999. Progressive parenchymal deposition of beta-amyloid precursor protein in rat brain following global cerebral ischemia. Acta. Neuropathol. 97, 359–368.

Lin, S., Cox, H., Rhodes, P., Cai, Z., 2006. Neuroprotection of alpha-phenyl-n-tert-butyl-nitrone on the neonatal white matter is associated with anti-inflammation. Neurosci. Lett. 405, 52–56.

Marcoux, F., Morawetz, R., Crowell, R., DeGirolami, U., Halsey, J.J., 1982. Differential regional vulnerability in transient focal cerebral ischemia. Stroke 13, 339–346.

Mattson, M., 1998. Modification of ion homeostasis by lipid peroxidation: roles in neuronal degeneration and adaptive plasticity. Trends Neurosci. 21, 53–57.

Matus, A., 1988. Microtubule-associated proteins: their potential role in determining neuronal morphology. Annu. Rev. Neurosci. 11, 29–44.

Miyamoto, E., Tomimoto, H., Nakao, S., Wakita, H., Akiguchi, I., Miyamoto, K., Shingu, K., 2001. Caudoputamen is damaged

by hypocapnia during mechanical ventilation in a rat model of chronic cerebral hypoperfusion. Stroke 32, 2920–2925.
Neumar, R., Bircher, N., Sim, K., Xiao, F., Zadach, K., Radovsky, A., Katz, L., Ebmeyer, E., Safar, P., 1995. Epinephrine and sodium bicarbonate during CPR following asphyxial cardiac arrest in rats. Resuscitation 29, 249–263.
Otani, H., Togashi, H., Jesmin, S., Sakuma, I., Yamaguchi, T., Matsumoto, M., Kakehata, H., Yoshioka, M., 2005. Temporal effects of edaravone, a free radical scavenger, on transient ischemia-induced neuronal dysfunction in the rat hippocampus. Eur. J. Pharmacol. 512, 129–137.
Pantoni, L., Garcia, J., 1997. Pathogenesis of leukoaraiosis: a review. Stroke 28, 652–659.
Pantoni, L., Garcia, J., Gutierrez, J., 1996. Cerebral white matter is highly vulnerable to ischemia. Stroke 27, 1641–1646 discussion 1647.
Petito, C., Feldmann, E., Pulsinelli, W., Plum, F., 1987. Delayed hippocampal damage in humans following cardiorespiratory arrest. Neurology 37, 1281–1286.
Pulsinelli, W., Brierley, J., Plum, F., 1982. Temporal profile of neuronal damage in a model of transient forebrain ischemia. Ann. Neurol. 11, 491–498.
van Groen, T., Puurunen, K., Mäki, H., Sivenius, J., Jolkkonen, J., 2005. Transformation of diffuse beta-amyloid precursor protein and beta-amyloid deposits to plaques in the thalamus after transient occlusion of the middle cerebral artery in rats. Stroke 36, 1551–1556.
Vargas, M., Barres, B., 2007. Why is Wallerian degeneration in the CNS so slow? Annu. Rev. Neurosci. 30, 153–179.
Watanabe, T., Yuki, S., Egawa, M., Nishi, H., 1994. Protective effects of MCI-186 on cerebral ischemia: possible involvement of free radical scavenging and antioxidant actions. J. Pharmacol. Exp. Ther. 268, 1597–1604.
Yam, P., Dewar, D., McCulloch, J., 1998. Axonal injury caused by focal cerebral ischemia in the rat. J. Neurotrauma. 15, 441–450.
Yam, P., Dunn, L., Graham, D., Dewar, D., McCulloch, J., 2000. NMDA receptor blockade fails to alter axonal injury in focal cerebral ischemia. J. Cereb. Blood Flow Metab. 20, 772–779.
Yamamoto, T., Yuki, S., Watanabe, T., Mitsuka, M., Saito, K., Kogure, K., 1997. Delayed neuronal death prevented by inhibition of increased hydroxyl radical formation in a transient cerebral ischemia. Brain Res. 762, 240–242.
Yoneda, Y., Uehara, T., Yamasaki, H., Kita, Y., Tabuchi, M., Mori, E., 2003. Hospital-based study of the care and cost of acute ischemic stroke in Japan. Stroke 34, 718–724.

BRAIN RESEARCH 1203 (2008) 170–176

available at www.sciencedirect.com

ScienceDirect

www.elsevier.com/locate/brainres

BRAIN RESEARCH

Research Report

Cilostazol alleviates cerebral small-vessel pathology and white-matter lesions in stroke-prone spontaneously hypertensive rats

Youshi Fujita, J-Xi Lin, Ryosuke Takahashi, Hidekazu Tomimoto*

Department of Neurology, Graduate School of Medicine, Kyoto University, 54 Kawaharamachi, Shogoin, Sakyo-ku, Kyoto 606-8507, Japan

ARTICLE INFO

Article history:
Accepted 29 January 2008
Available online 19 February 2008

Keywords:
Small-vessel disease
White matter
Stroke-prone spontaneously hypertensive rat
Vascular smooth-muscle cell
Phenotypic modulation
Cilostazol

ABSTRACT

Small-vessel pathology is believed to have a critical role in cerebrovascular white-matter (WM) lesions. However, the cellular aspect of vascular pathology, including the phenotypic modulation of smooth-muscle cells (SMCs) and its role in the small-vessel disease, remains undefined. The involvement or otherwise of the phenotypic modulation of SMCs in cerebral small-vessel pathology has been investigated, and the effect of cilostazol on both the small vessels and the WM lesions has been determined in stroke-prone spontaneously hypertensive rats (SHRSP). Male SHRSP and Wistar Kyoto rats were used. SHRSP were divided into two groups: the cilostazol-treated (20-week treatment) and vehicle-treated groups. Small-vessel pathology was analyzed using both histopathology and immunohistochemistry for smooth-muscle actin and nonmuscle myosin heavy chain (SMemb, a marker for the synthetic phenotype of SMC). The pathological changes in the WM were quantified in terms of the numerical density of activated microglia and the degree of WM lesions. Vascular wall thickening and perivascular fibrosis, determined by the wall area/lumen area ratio and the collagen area/total vessel area ratio, respectively, showed an increase in the vehicle-treated SHRSP, and this increase was significantly attenuated by cilostazol treatment. The percentage of small vessels immunopositive for SMemb was also reduced by cilostazol treatment. In the cilostazol-treated SHRSP, microglial activation and the degree of WM lesions were attenuated compared with the vehicle-treated SHRSP. The results indicated that cilostazol attenuates the phenotypic modulation of SMC associated with cerebral small-vessel pathology and WM lesions without causing changes in the blood pressure.

1. Introduction

Cerebral small-vessel disease has a central role in the pathogenesis of subcortical vascular dementia (SVD), with hypertension as the important risk factor (van Swieten et al., 1991; Pantoni and Garcia, 1995; Kalaria et al., 2004). SVD, a major subtype of vascular dementia, is pathologically characterized by multiple lacunae and widespread white-matter (WM) lesions (Roman et al., 2002; Yanagihara, 2002). These lesions are attributed to the occlusion or stenosis of medullary or lenticulostriate arteries, which penetrate and distribute themselves in the subcortical WM (Fisher, 1968; Lin et al., 2000).

* *Corresponding author*. Fax: +81 075 751 3766.
E-mail address: fujitauc@kuhp.kyoto-u.ac.jp (Y. Fujita).

Abbreviations: SVD, subcortical vascular dementia; WM, white matter; SMC, smooth-muscle cells; SHRSP, Stroke-prone spontaneously hypertensive rats; WKY, Wistar Kyoto; TNF-α, tumor necrosis factor alpha

0006-8993/$ – see front matter © 2008 Elsevier B.V. All rights reserved.
doi:10.1016/j.brainres.2008.01.103

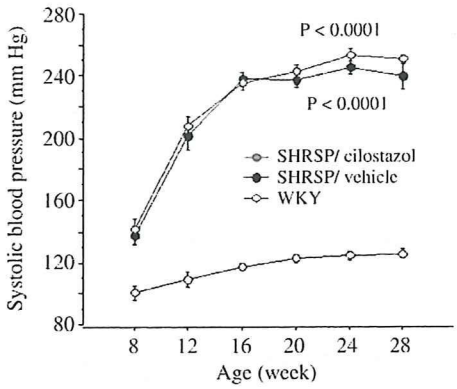

Fig. 1 – Systolic blood pressure in the three groups of rats during the treatment period. $p<0.0001$ vs WKY.

Structural change or vascular remodeling occurs primarily in small resistance arteries and arterioles in chronic hypertension (Baumbach and Heistad, 1989). The changes include luminal narrowing and wall thickening, processes in which the vascular smooth-muscle cells (SMCs) and the extracellular matrix are involved (Johansson and Fredriksson, 1985). Vascular remodeling involves the phenotypic modulation of SMCs from physiological contractile phenotype to pathophysiological synthetic phenotype (Contard et al., 1993; Pauletto et al., 1995). The phenotype was defined originally on the basis of ultrastructural features (Chamley-Campbell et al., 1979) and subsequently on the basis of the changes in their phenotypic markers, including nonmuscle myosin heavy chain-B (SMemb) (Aikawa et al., 1993). The synthetic phenotype is characterized by a decrease in contractile capacity combined with active proliferation (Kocher et al., 1991) and motility (Grünwald and Haudenschild, 1984), production of extracellular matrices such as collagen (Sjolund et al., 1986). Phenotypic modulation of SMCs plays a pivotal role in atherosclerosis and restenosis after angioplasty (Aikawa et al., 1997), and it also has been shown to involve the small vessels of the heart and skeletal muscles in chronic hypertension (Contard et al., 1993; Puato et al., 2004). However, the role of phenotypic modulation of SMCs remains undefined in SVD.

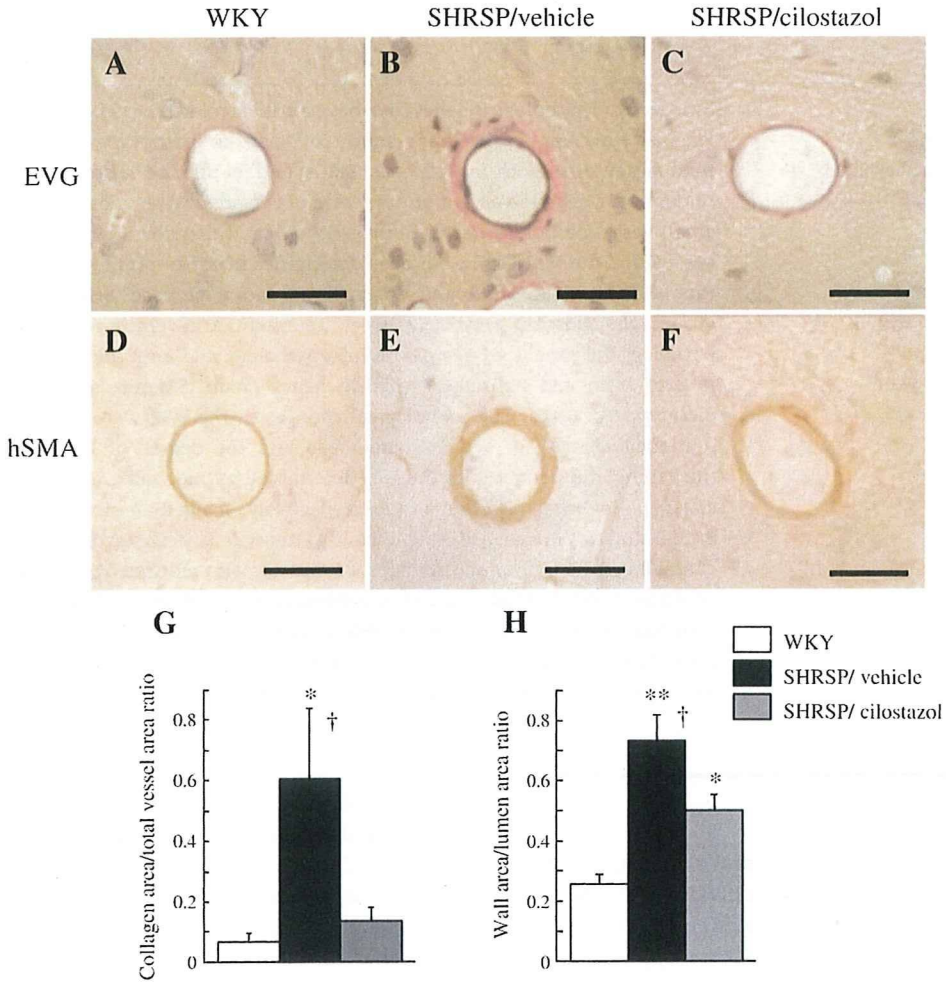

Fig. 2 – Representative photomicrographs of cross-sections of cerebral small vessels from the WKY (A, D), vehicle-treated SHRSP (B, E), and cilostazol-treated SHRSP groups (C, F). The sections were stained with elastica van Gieson's stain (A, B and C) and immunohistochemistry for hSMA (D, E and F). Collagen is stained red with elastica van Gieson's stain (B). Increased perivascular collagen deposition and wall thickening are apparent in vehicle-treated SHRSP (B, E). Bars indicate 30 μm. Bar graphs indicate collagen area/total vessel area ratio (G) and wall area/lumen area ratio (H). *$p<0.05$; **$p<0.01$ vs the WKY. †$p<0.05$ vs the cilostazol-treated SHRSP.

Cilostazol has been known as an antithrombotic and vasodilating drug (Dawson et al., 1998), which increases the intracellular cAMP by inhibiting phosphodiesterase type III (Kimura et al., 1985). In a recent clinical trial, treatment with cilostazol has been found to reduce the risk of recurrent stroke, especially in patients with lacunar infarction, suggesting that cilostazol has a specific effect against small-vessel disease (Gotoh et al., 2000). Meanwhile, a recent in vitro study has shown that an increase in the intracellular cAMP level induces the differentiation of SMCs from the synthetic phenotype to the contractile phenotype (Fetalvero et al., 2006). These findings have led us to suggest that cilostazol attenuates the phenotypic modulation associated with small-vessel remodeling and WM lesions in vivo.

Stroke-prone spontaneously hypertensive rats (SHRSP) provide an excellent model for SVD accompanied by small-vessel pathology, because these rats show chronic hypertension, structural alterations of small cerebral arteries (Fredriksson et al., 1988), reduction in cerebral blood flow (Yamori and Horie, 1977; Katayama et al., 1997), WM lesions (Hazama et al., 1995; Lin et al., 2001), and cognitive impairment (Saito et al., 1995). In the present study, the occurrence or otherwise of phenotypic modulation of SMCs in the cerebral small vessels has been investigated, and furthermore, the suppression of both pathological vascular changes and WM lesions in SHRSP by cilostazol has been determined.

2. Results

2.1. *Physiological parameter*

The systolic blood pressure was significantly higher in SHRSP than in Wistar Kyoto (WKY) rats ($p<0.0001$). However, there was no significant difference in the blood pressure between the vehicle-treated SHRSP and cilostazol-treated SHRSP (Fig. 1).

2.2. *Structural changes in the small vessels*

Collagen area/total vessel area ratio was significantly higher in the vehicle-treated SHRSP than in the WKY rats and cilostazol-treated SHRSP (Fig. 2A–C and G). The medial cross-sectional area in the sections immunostained for human smooth-muscle actin (hSMA) was also larger in the vehicle-treated SHRSP than in the WKY rats and cilostazol-treated SHRSP (Fig. 2D–F). As shown in Fig. 2H, wall area/lumen area ratio was significantly higher in the vehicle-treated SHRSP compared with the WKY rats, and this pathological change was significantly attenuated by cilostazol treatment, although it still remained higher than the WKY rats.

2.3. *Expression of SMemb in the cerebral small vessels*

The percentage of small vessels immunopositive for SMemb showed a significant increase in the vehicle-treated SHRSP than in the WKY rats, and cilostazol treatment suppressed the expression of this protein, although the percentage still remained increased compared with the WKY rats (Fig. 3A–D).

2.4. *White-matter lesions*

Grading scores for the WM lesions were significantly higher in the vehicle-treated SHRSP than in the WKY rats. Cilostazol significantly ameliorated WM lesions compared with the vehicle-treated SHRSP (Fig. 4A–C and G). Major histocompatibility complex (MHC) class II-immunopositive microglia showed an increase in the WM of the vehicle-treated SHRSP, and this

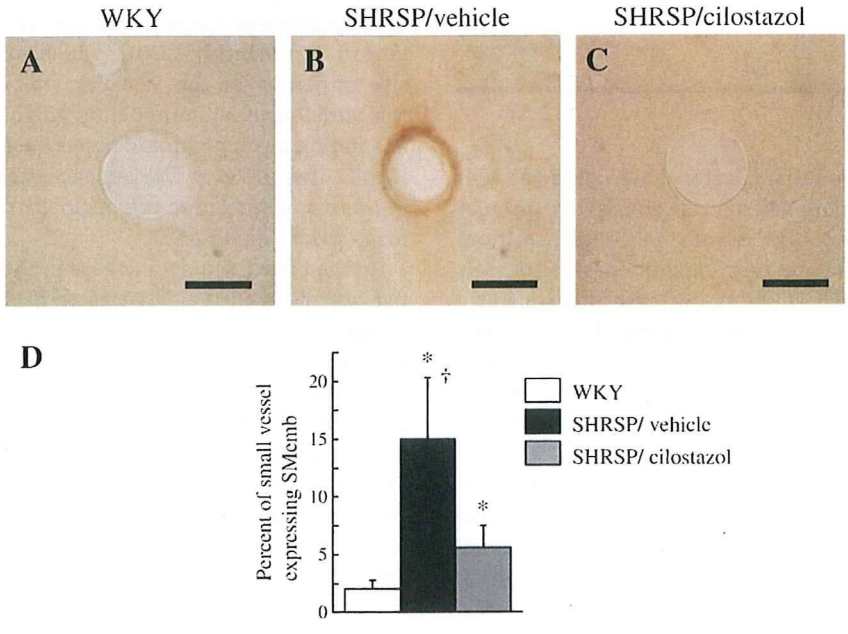

Fig. 3 – Immunohistochemical staining for SMemb in the small vessel from WKY (A), vehicle-treated SHRSP (B), and cilostazol-treated SHRSP (C) groups. Bars indicate 30 μm. Bar graph indicates the percentage of small vessels expressing SMemb (D). *$p<0.05$ vs the WKY. †$p<0.05$ vs the cilostazol-treated SHRSP.

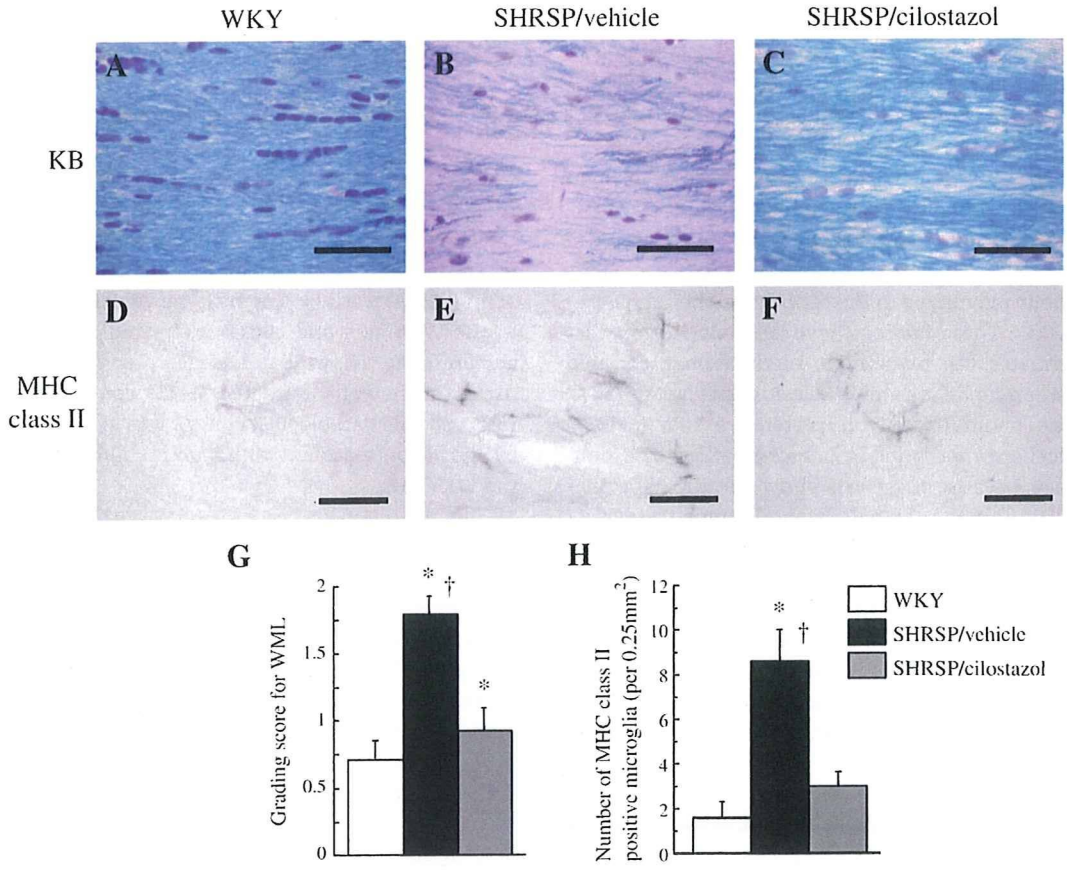

Fig. 4 – Photomicrographs of Klüver–Barrera staining of the WM (A, B, and C) and immunohistochemical staining for MHC class II (D, E, and F) in the WKY, vehicle-treated SHRSP, and cilostazol-treated SHRSP groups. Bar graphs indicate the grading score for WM lesions and the number of MHC class II-positive cells in the WM (G and H, respectively). Bars indicate 30 μm (A, B, and C) and 50 μm (D, E, and F). *$p<0.05$ vs the WKY and †$p<0.05$ vs the cilostazol-treated SHRSP.

increase was significantly attenuated by cilostazol treatment (Fig. 4D–F and H).

3. Discussion

The present study showed that cilostazol alleviated vascular remodeling, including small-arterial thickening, perivascular collagen deposition, and WM lesions in SHRSP, without affecting the arterial blood pressure. In addition, small vessels expressing SMemb showed a numeric decrease after cilostazol treatment in SHRSP. These findings supported the hypothesis that cilostazol attenuated the phenotypic modulation of SMCs from the contractile phenotype toward the synthetic phenotype, which might contribute to the production of collagen and morphological changes of the vascular wall.

In accordance with previous studies (Baumbach and Heistad, 1989; Hart et al., 1980), narrowing of the vascular lumen and an increase in the wall area/lumen area ratio in the small cerebral arteries of SHRSP were observed. A recent clinical study has shown that an increased wall area/lumen area ratio of subcutaneous small resistance arteries was one of the most potent predictors for cardiovascular event in patients with hypertension (Rizzoni et al., 2003). Therefore, structural changes in small arteries might be causally related to ischemic organ damage. Vascular remodeling in hypertension involves the deposition of extracellular matrix, especially collagen (Intengan and Schiffrin, 2001), which might induce a progressive stiffening of the vascular wall. In the earlier stages, this small-arterial remodeling might reflect physiological adaptation against chronic hypertension (Owens et al., 2004; Cipolla et al., 2006); however, excessive structural alterations in the microcirculation might finally contribute to organ damage (Izzard et al., 2005).

In the present study, increase in the SMemb-immunopositive vessels in the vehicle-treated SHRSP indicated that phenotypic modulation accompanied vascular wall thickening and perivascular collagen deposition. The role of phenotypic modulation of SMCs in the process of vascular remodeling is poorly understood; however, it might, at least in part, contribute to pathological vascular remodeling. Vascular SMC has unique properties, enabling it to show various stages of its phenotypes, ranging from the highly synthetic and immature phenotype to the highly contractile and mature phenotype, depending on the respective environmental cues (Owens et al., 2004). Although little is understood about the mechanisms regulating phenotypic modulation of SMC in vivo (Izzard et al., 2005), a recent study has indicated the beneficial effect of the increase in intracellular cAMP, which promoted differentiation of SMC from the synthetic to the contractile phenotype in vitro